Development of Novel Water-Gas-Shift Membrane Reactor

W.S. Winston Ho, Professor
Department of Chemical and Biomolecular Engineering
Department of Materials Science and Engineering
The Ohio State University
2041 College Road
Columbus, OH 43210-1178
(614) 292-9970; fax: (614) 292-3769; e-mail: ho@che.eng.ohio-state.edu

DOE Technology Development Manager: Dr. Amy Manheim
(202) 586-1507; e-mail: Amy.Manheim@ee.doe.gov

DOE Field Project Officer: Reginald Tyler
(303) 275-4929; fax: (303) 275-4753; e-mail: reginald.tyler@go.doe.gov

ANL Technical Advisor: Thomas G. Benjamin
(630) 252-1632; fax: (630) 252-4176; e-mail: benjamin@cmt.anl.gov

Contract/Grant No. DE-FC36-03AL68510, The Ohio State University, 08/16/2002 – 09/30/2004

Contract/Grant No. DE-FC04-01AL67629, University of Kentucky, 10/01/2001 – 08/15/2002

Abstract

This report summarizes the objectives, technical barrier, approach, and accomplishments for the development of a novel water-gas-shift (WGS) membrane reactor for hydrogen enhancement and CO reduction. We have synthesized novel CO_2-selective membranes with high CO_2 permeabilities and high CO_2/H_2 and CO_2/CO selectivities by incorporating amino groups in polymer networks. We have also developed a one-dimensional non-isothermal model for the countercurrent WGS membrane reactor. The modeling results have shown that H_2 enhancement (>99.6% H_2 for the steam reforming of methane and >54% H_2 for the autothermal reforming of gasoline with air on a dry basis) via CO_2 removal and CO reduction to 10 ppm or lower are achievable for synthesis gases. With this model, we have elucidated the effects of system parameters, including CO_2/H_2 selectivity, CO_2 permeability, sweep/feed flow rate ratio, feed temperature, sweep temperature, feed pressure, catalyst activity, and feed CO concentration, on the membrane reactor performance. Based on the modeling study using the membrane data obtained, we showed the feasibility of achieving H_2 enhancement via CO_2 removal, CO reduction to ≤ 10 ppm, and high H_2 recovery. Using the membrane synthesized, we have obtained <10 ppm CO in the H_2 product in WGS membrane reactor experiments. From the experiments, we verified the model developed. In addition, we removed CO_2 from a syngas containing 17% CO_2 to about 30 ppm. The CO_2 removal data agreed well with the model developed. The syngas with about 0.1% CO_2 and 1% CO was processed to convert the carbon oxides to methane via methanation to obtain <5 ppm CO in the H_2 product.

Objectives

- Produce a hydrogen product with <10 ppm CO at the high pressure used for reforming.
- Overcome Fuel-Flexible Fuel Processors Barrier L: H_2 purification/CO clean-up.
- Synthesize and characterize CO_2-selective membranes for the novel WGS membrane reactor.
- Develop the water-gas-shift (WGS) membrane reactor for achieving <10 ppm CO.
- Develop and verify a mathematical model to predict the performance of the WGS membrane reactor.

Technical Barrier
The Hydrogen, Fuel Cells and Infrastructure Technologies Multiyear Research, Development and Demonstration Plan technical barrier this project addressed included:

- L: H_2 Purification/CO Clean-up (to achieve the target of <10 ppm CO).

Approach

- Synthesize and characterize CO_2-selective membranes containing amino groups.
- Use the CO_2-selective membrane synthesized to remove CO_2 for H_2 enhancement.
- Drive the WGS reaction to the product side via CO_2 removal:
  $CO + H_2O \rightarrow H_2 + CO_2\uparrow$
- Decrease CO to <10 ppm in the H_2 product via CO_2 removal.
- Develop a mathematical model to predict the performance of the membrane reactor.
- Use the model developed to study membrane reactor performance and to guide/minimize experimental work.

Accomplishments

- Obtained <10 ppm CO in the H_2 product in WGS membrane reactor experiments using the small circular lab membrane cell ("Small Cell") with the syngas feed with 1% CO. Confirmed the <10 ppm CO result using the "Big Cell" WGS membrane reactor in the rectangular flat-sheet shape with well-defined flow that had 7.5 times the membrane area of "Small Cell". This achieved the project milestone of <10 ppm CO in the H_2 product.
- The data from the "Big Cell" WGS membrane reactor agreed well with the mathematical model developed. The data and model can be used for the reactor scale-up.
- Synthesized membranes with high CO_2 permeabilities and high CO_2/H_2 and CO_2/CO selectivities.
- Developed a one-dimensional non-isothermal model for the countercurrent WGS membrane reactor to predict performance and guide/minimize experimental effort.
- Removed CO_2 from a syngas containing 17% CO_2 to about 30 ppm. The CO_2 removal data agreed well with the mathematical model developed. The syngas with about 0.1% CO_2 and 1% CO was processed to convert the carbon oxides to methane via methanation to obtain <5 ppm CO in the H_2 product.

Introduction

A water gas shift (WGS) reactor for the conversion of carbon monoxide (CO) and water to hydrogen (H_2) and carbon dioxide (CO_2) is widely used in chemical and petroleum industries.

The reactor is also critically needed for the conversion of fuels, including gasoline, diesel, methanol, ethanol, natural gas, biomass, and coal, to H_2 for fuel cells. Since the WGS reaction is reversible, it is not efficient, resulting in a high concentration of unconverted CO (~ 1%) in the H_2 product and a bulky, heavy reactor. The reversible, exothermic WGS reaction is as follows:

$$CO(g) + H_2O(g) \leftrightarrow CO_2(g) + H_2(g) \qquad \Delta H_r = -41.1 \quad kJ / mol \qquad (1)$$

where ΔH_r is the heat of reaction. This reaction can be enhanced significantly through a CO_2-selective or H_2-selective membrane, which removes one of the reaction products, CO_2 or H_2, respectively, to beat the reaction equilibrium and shift the reaction towards the product side.

Using a CO_2-selective membrane [1, 2] with the continuous removal of CO_2, a CO_2-selective WGS membrane reactor is a promising approach to enhance CO conversion and increase the purity of H_2 under relatively low temperatures (~150^oC). In comparison with the H_2-selective membrane reactor, the CO_2-selective WGS membrane reactor is more advantageous because (1) a high-purity H_2 product is recovered at the high pressure (feed gas pressure) and (2) air or an inert gas can be used as the sweep gas to remove the permeate, CO_2, on the low-pressure side of the membrane to have a high driving force for the separation. These advantages are especially important for fuel cell vehicles. The first advantage eliminates the need for an unwanted compressor. With the second advantage, the high driving force created by the sweep gas can result in low CO concentration and high H_2 purity and recovery. Several studies have been done on H_2-selective membrane reactors, mainly based on palladium membranes and using high-temperature WGS catalysts [3-8].

We have synthesized novel CO_2-selective polymer membranes containing amino groups with high CO_2 permeabilities and high CO_2/H_2 and CO_2/CO selectivities [9]. We have also developed a mathematical model [10-12] to predict the performance of the WGS membrane reactor and to guide and minimize experimental efforts on the reactor. With the modeling and experimental efforts, we have obtained <10 ppm CO in the H_2 product using two WGS membrane reactors in different size. In other words, we have achieved the project milestone of <10 ppm CO in the H_2 product. In addition, we removed CO_2 from a syngas containing 17% CO_2 to about 30 ppm. The treated syngas with such a low CO_2 concentration was readily processed to convert the carbon oxides to methane via methanation to obtain <5 ppm CO in the H_2 product.

Approach

We have synthesized novel CO_2-selective membranes with high CO_2 permeabilities and high CO_2/H_2 and CO_2/CO selectivitie by incorporating amino groups in polymer networks. We incorporated the membrane synthesized in the WGS membrane reactors to show CO reduction to 10 ppm or lower in the H_2 product in reactor experiments using the synthesis gas feed with 1% CO. We have developed a mathematical model [10-12] to predict the performance of the WGS membrane reactor and to guide and minimize experimental efforts on the reactor. In the model, the low-temperature WGS reaction kinetics for the commercial catalyst ($Cu/ZnO/Al_2O_3$) reported by Moe [13] and Keiski et al. [14] was used. We verified the model for the prediction of the performance of the "Big Cell" WGS membrane reactor. In addition, we used the membrane synthesized to remove CO_2 from syngas for H_2 purification via methanation.

Results and Discussion

The results on synthesis and characterization of novel CO_2-selective membranes, modeling of membrane reactor, laboratory membrane reactor ("Small Cell") experiments, "Big Cell" membrane reactor experiments, effective removal of CO_2 from syngas, and methanation of treated syngas to achieve <10 ppm CO are discussed in the following paragraphs.

Synthesis and Characterization of Novel CO_2-Selective Membranes

We have synthesized novel CO_2-selective membranes by incorporating amino groups in polymer networks. The membranes consisted of crosslinked polymers and aminoacid salts. The polymers included polyimide, polyvinylalcohol, and polyamines (polyethylenimine and polyallylamine), and the aminoacid salts were the lithium, sodium, potassium and aluminum salts of N,N-dimethylglycine, glycine, and 2-aminoisobutyric acid. The polyamines and the aminoacid salts were the fixed and mobile carriers for the transport of CO_2 across the membrane. The membranes were prepared by casting a solution containing the polymer, polyamine and aminoacid salt onto a microporous support. The thickness of the membrane was controlled by using a GARDCO adjustable micrometer film applicator (Paul N. Gardner Company, Inc., Pompano Beach, FL). Figure 1 shows the scanning electron microscopic picture of the membrane synthesized on a microporous support. As shown in this figure, the nonporous membrane was about 20 micron thick, and the microporous support was about 80 micron thick. The membrane is based on the facilitated transport mechanism [1, 2, 9, 15], in which CO_2 transfer through the membrane is enhanced via reaction with amino groups in the membrane, and H_2 and CO are rejected by the membrane due to the absence of reaction.

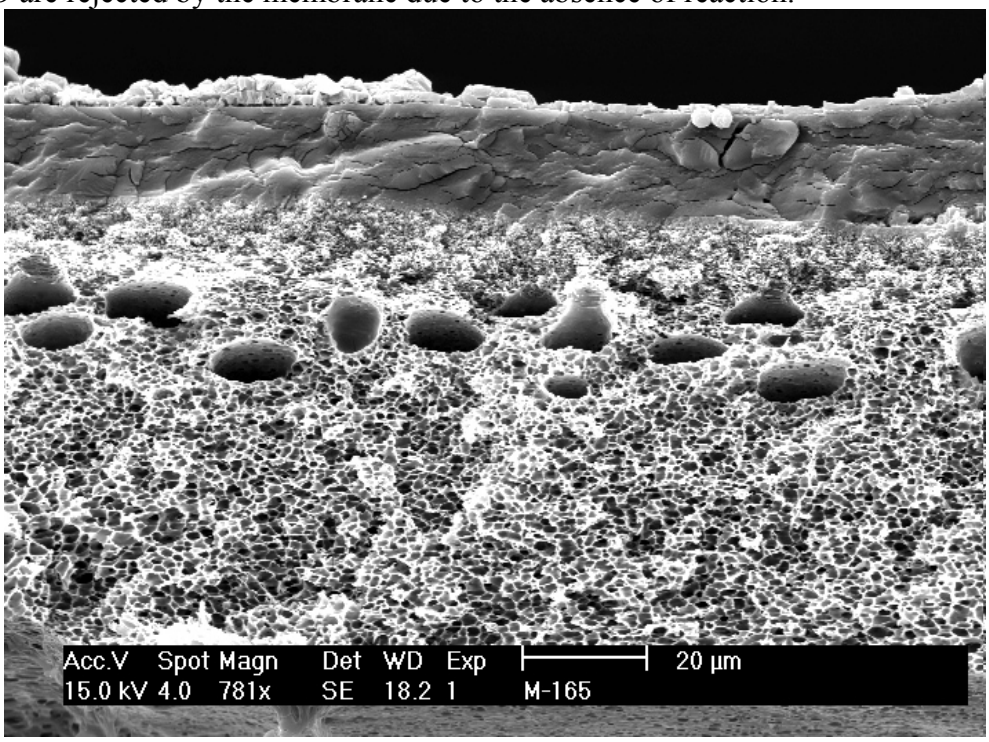

Figure 1. Scanning electron microscopic picture of the membrane synthesized.

The membranes synthesized were characterized in a gas permeation unit to determine their CO_2 permeabilities and CO_2/H_2 and CO_2/CO selectivities. Figure 2 shows the schematic of the gas permeation unit equipped with a computerized data acquisition system and a gas chromatograph. The gas streams were analyzed with an Agilent 6890N gas chromatograph (GC) (Agilent Technologies, Palo Alto, CA) with two thermal conductivity detectors using argon and helium as carrier gases, respectively. The volume of sampling loop of GC was 0.25 ml. The GC column used was a micro-packed column Carboxen 1040, 3 ft long with a diameter of 1/16 inch from SUPELCO, Bellefonte, PA. Two feed gases with certified compositions were used; one consisted of 20% CO_2, 40% H_2, and 40% N_2, and the other had 17% CO_2, 1.0% CO, 45% H_2, and 37% N_2. The second composition was used to simulate the composition of synthesis gas from autothemal reforming with air. Argon or air was used as the sweep gas. Gas flow rates were controlled by mass flow meters from Brooks Instrument, Hatfield, PA. The feed gas and the sweep gas were passed countercurrently through the membrane permeation cell. Water was pumped into both compartments of the membrane cell to control the water contents of the feed and sweep gases. For the permeability and selectivity measurements, a circular flat-sheet membrane cell (with a membrane area of 45.60 cm^2) was used.

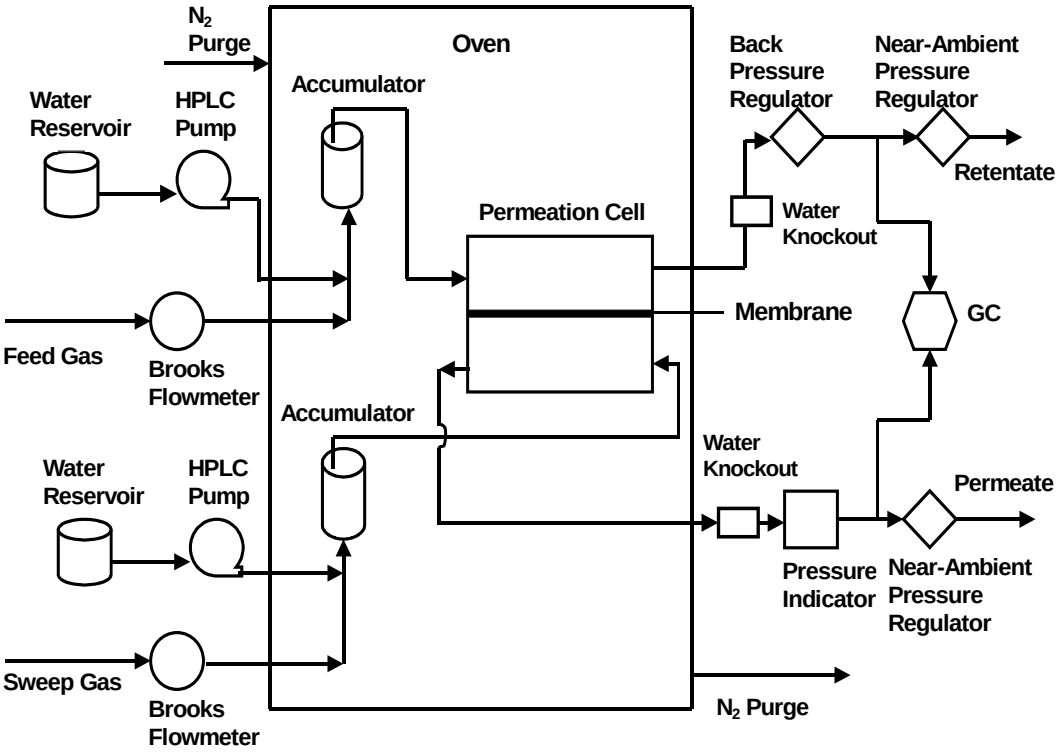

Figure 2. The schematic of the gas permeation unit.

Figure 3 gives the CO_2 permeability and CO_2/H_2 selectivity results as a function of temperature from 100°C to 180°C for the feed gas pressure of 2.1 atm and the sweep gas (air or nitrogen) of atmospheric pressure. As shown in this figure, the CO_2 permeability was about 4000 Barrers (1 Barrer = 10^{-10} cm^3(STP)-cm/cm^2-s-cmHg) or higher for the temperatures ranging from 100°C to 150°C. However, the permeability reduced to about 2000 Barrers as the temperature increased to 180°C. This was due to the reduction of water retention in the membrane as the temperature

increased. Also shown in this figure, the CO_2/H_2 selectivity was about 100 or higher for the temperatures ranging from 100°C to 150°C. However, the selectivity reduced slightly as the temperature increased to 170°C. This was a result of CO_2 permeability decrease due to the reduction of water retention in the membrane described above. At 180°C, the selectivity reduced significantly to slightly greater than 10 due to the significant swelling of this membrane at this high temperature. Nonetheless, the selectivity of 10 is still good enough to give a reasonably high H_2 recovery of about 90%, which will be described in the following modeling work.

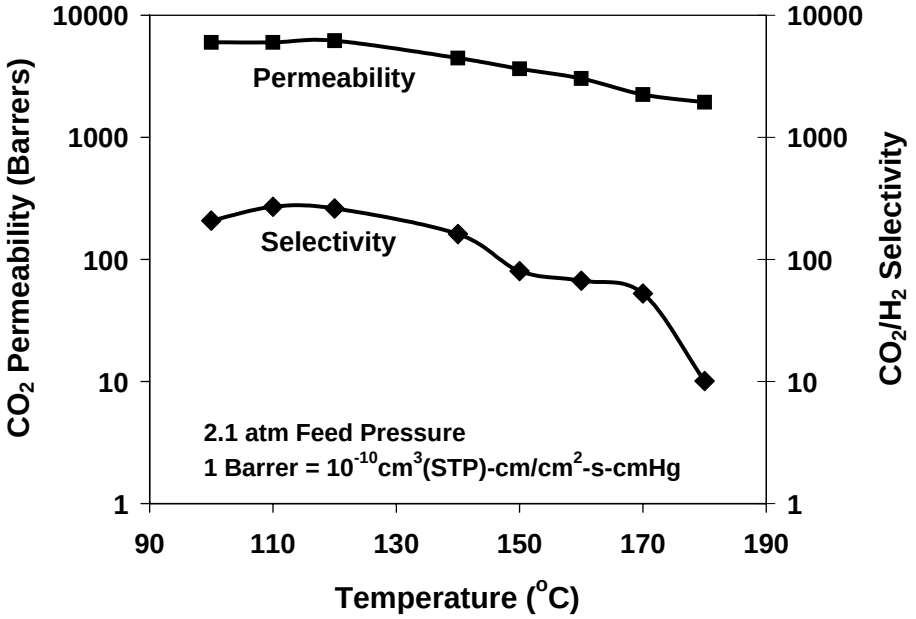

Figure 3. CO_2 permeability and CO_2/H_2 selectivity results as a function of temperature.

Figure 4 gives the CO_2 permeability results as a function of feed pressure from about 2 atm to about 4 atm at 150°C. As shown in this figure, the permeability did not change significantly with the feed pressure.

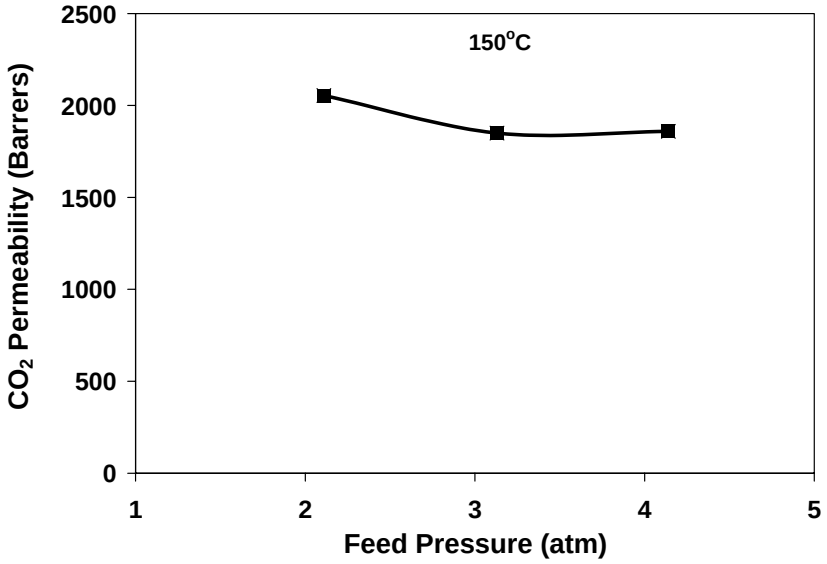

Figure 4. CO_2 permeability results as a function of feed pressure at 150°C.

Figure 5 depicts the CO_2/CO selectivity results as a function of temperature from 100°C to 160°C for the feed gas pressure of 2.1 atm. The CO_2/CO selectivity results for this temperature range were greater than 215, which is very good. However, the selectivity reduced as the temperature increased. This was a result of CO_2 permeability decrease due to the reduction of water retention in the membrane described above.

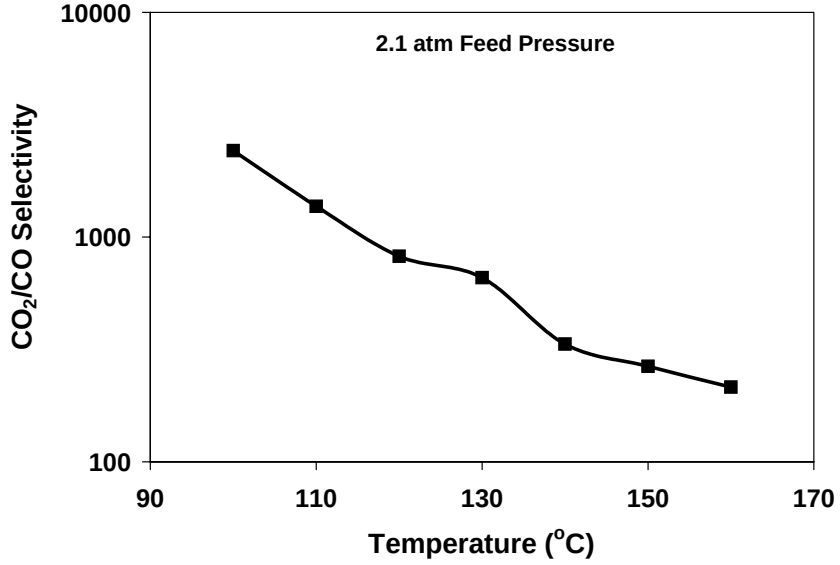

Figure 5. CO_2/CO selectivity results as a function of temperature.

Modeling of Membrane Reactor

Model Development

As one of the two main types of commercialized membrane modules, the hollow fiber membrane module has shown excellent mass transfer performance because of its large surface area per unit volume (about 3000 ft^2/ft^3 for gas separation) [15]. In this modeling work, the WGS membrane reactor was configured to be a hollow fiber membrane module with catalyst particles packed inside the fibers. The following assumptions were made in the model:

(1) The hollow fiber module is composed of CO_2-selective facilitated transport membrane;
(2) CO_2 and H_2 are the only two gases permeating through the membrane;
(3) Membrane permeability is fixed and does not change with temperature variation in the module;
(4) There is no temperature variation in the radial direction inside a hollow fiber due to its small dimension;
(5) The module is adiabatic and operating at a steady state;
(6) There is no axial mixing;
(7) The pressure drops on both lumen and shell sides are negligible.

The CO_2 permeability of the membrane was in the range of 1000 to 8000 Barrers (1 Barrer = 10^{-10} cm^3 (STP) • cm/cm^2 • s • cm Hg), and the CO_2/H_2 selectivity, expressed in Eq. (2) [15], was in the range of 10 to 80.

$$\alpha = \frac{y_{CO_2} / y_{H_2}}{x_{CO_2} / x_{H_2}} \tag{2}$$

The catalyst packed was assumed to be the commercial Cu/ZnO catalyst for lower-temperature WGS reaction. A number of studies on the reaction kinetics of the commercial WGS catalyst, $CuO/ZnO/Al_2O_3$, have been published [13, 14, 16-19]. Above 200°C, Campbell's [16] rate equation is pore-diffusion limited, not chemical-reaction limited. Campbell stated that his reaction rate fitted poorly with experimental data obtained for temperatures less than 200°C. Fiolitakis et al. [17] gave an activation energy of 46 kJ/mol but did not give a reaction rate constant. Salmi and Hakkarainen [18] only had data for temperatures greater than 200°C. Based on the experimental data of the commercial catalyst (ICI 52-1), Keiski et al. [14] gave two reaction rates for the low-temperature WGS reaction over a range of 160 – 250°C. The first was dependent only on CO concentration and gave an activation energy of 46.2 kJ/mol. The second reaction rate was dependent on CO and steam concentrations with a lower activation energy of 42.6 kJ/mol. Because of the proximity of our operation conditions to theirs and the fact that steam is in excess in most of the membrane reactors, Keiski et al.'s first reaction rate expression was chosen for this work. The reaction rate is given by Eq. (3).

$$r_i = 1.0 \times 10^{-3} \frac{\rho_b p_f}{n_t R T_f} \exp(13.39 - \frac{5557}{T_f}) n_{CO} (1 - \frac{n_{f,H_2} n_{f,CO_2}}{K_T n_{f,CO} n_{f,H_2O}}) \tag{3}$$

where the expression for K_T [13, 14] is as follows:

$$K_T = \exp(-4.33 + \frac{4577.8}{T_f}) \tag{4}$$

The temperatures of both feed (lumen) and sweep (shell) sides are affected by the heat of the reaction and the heat transfer through the membrane. The overall heat transfer coefficient U_i was derived via the series resistance method to include both convective and conductive heat transfer.

$$U_i = \frac{1}{\frac{1}{h_f} + \frac{d_{in}}{2k_m} \ln(\frac{d_{in} + 2\ell}{d_{in}}) + \frac{d_{in}}{2[(1-\varepsilon)k_m + \varepsilon k_a]} \ln(\frac{d_{out}}{d_{in} + 2\ell}) + \frac{d_{in}}{d_{out}} \frac{1}{h_s}} \tag{5}$$

where h_f is the feed (lumen) side heat transfer coefficient, h_s is the sweep (shell) side heat transfer coefficient, ℓ is the effective thickness of the selective membrane layer (on the inside of the hollow fiber), k_m and k_a are the thermal conductivities of the membrane and the gas, respectively, ε is the porosity of the support layer of the hollow fiber, and d_{in} and d_{out} are the inside and outside diameters of the hollow fiber, respectively. In Eq. (5), the thermal conductivities of the selective membrane layer and the hollow-fiber support layer were assumed to be the same, i.e., k_m, which is true for an integrally skinned membrane [15].

The convective heat transfer for the feed (lumen) side can be considered to be that on the inside wall of a packed bed. Due to the small dimension of the lumen, we assumed that the inside heat

transfer resistance was negligible and then there was no temperature difference in the radical direction inside the fiber. Many researchers have studied the shell side mass transfer of hollow fiber modules based on either empirical or fundamental work [20-24]. According to the analogy between heat and mass transfer, similar equations can be used for the calculation of heat transfer coefficients by changing Sh to Nu and Sc to Pr, respectively. Yang and Cussler's correlation equation [20] was chosen because the module configuration and operation parameters they used were similar to those in this work.

$$h_s = 1.25 \frac{k_a}{d_h^{0.07}} \left(\frac{\mathrm{Re}}{L} \right)^{0.93} \mathrm{Pr}^{0.33} \qquad (6)$$

where d_h is the hydraulic diameter, L is the hollow fiber length, Re is the Reynolds number, and Pr is the Prandtl number. In addition, because mass transfer and heat transfer occurred simultaneously in the membrane reactor, the energy carried by permeating gases was also taken into account in the model.

Based on the schematic diagram of the WGS hollow-fiber membrane reactor illustrated in Figure 6, the molar and energy balances were performed on both feed (lumen) and sweep (shell) sides, respectively.

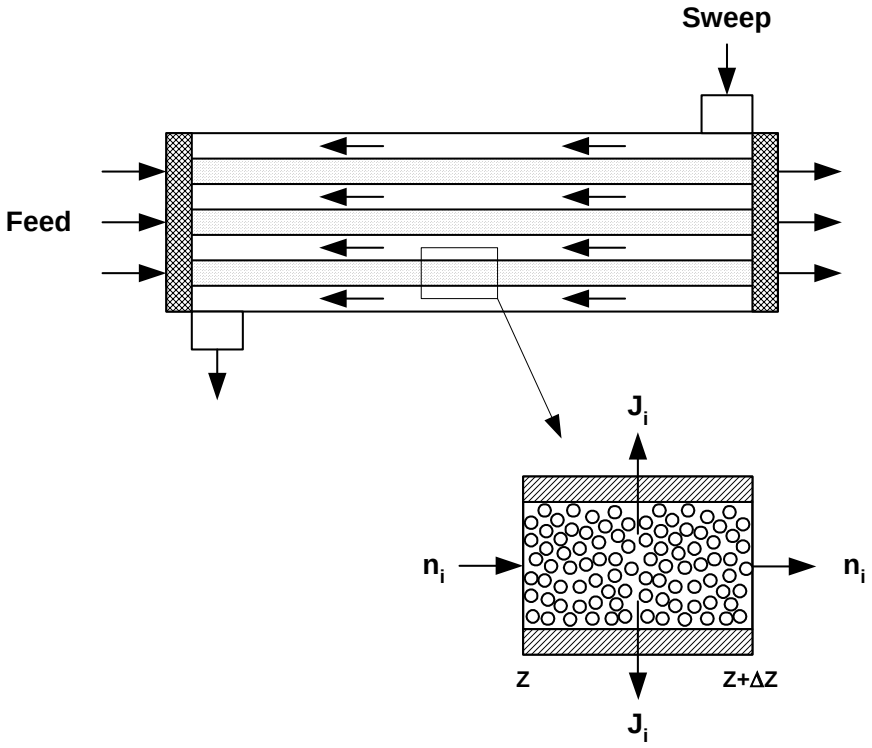

Figure 6. Schematic diagram of water-gas-shift hollow-fiber membrane reactor.

Molar Balance

Based on the volume element from z to $z + \Delta z$, the molar balance on the feed or lumen side for gas species i can be expressed as:

In – Out + Generation = Accumulation

or

$$n_{fi}\Big|_{z} - n_{fi}\Big|_{z+\Delta z} - \pi\, d\, \Delta z J_i + \frac{1}{4}\pi\, d^2\, \Delta z\, r_i = 0 \tag{7}$$

where n_i , J_i and r_i are the molar flow rate, permeation flux and reaction rate of gas species i, respectively; and

$$J_i = P_i \frac{\Delta p_i}{\ell} \tag{8}$$

where P_i and Δp_i are the membrane permeability and transmembrane partial pressure difference of gas species i, respectively.

Dividing both sides of equation (7) by Δz and taking the limit as $\Delta z \rightarrow 0$ give:

$$\frac{dn_{fi}}{dz} = \frac{1}{4}\pi\, d_{in}{}^2 r_i - \pi\, d_{in}\, J_i \tag{9}$$

Similarly, the molar balance on the sweep or shell side is carried out, and the resulting equation is:

$$\frac{dn_{si}}{dz} = -\pi\, d_{in}\, J_i \tag{10}$$

In addition, the H_2 recovery is defined as the ratio of the exit H_2 molar flow rate to the combination of the inlet H_2 and CO molar flow rates. All these flow rates are on the feed, lumen side.

Energy balance

Considering the heat of the reaction, the heat transfer through the membrane, and the energy carried by permeating gases, we carried out the energy balance on the volume element of the membrane reactor from z to $z + \Delta z$. Differential equations were obtained by taking the limit as $\Delta z \rightarrow 0$. The differential equation for the feed or lumen side is:

$$\frac{d\sum(n_{fi}\, c_{pfi} T_f)}{dz} = \frac{1}{4}\pi\, d_{in}{}^2\, r_i\, \Delta H_r\, T_f - \pi\, d_{in}\, (U_i + c_{p_{CO_2}} J_{CO_2} + c_{p_{H_2}} J_{H_2})\, \Delta T \tag{11}$$

where ΔH_r is the heat of reaction, and c_p is the heat capacity of the individual gas species in the gas mixture.

The differential equation for the sweep or shell side is:

$$\frac{d\sum(n_{si}\, c_{psi} T_s)}{dz} = -\pi\, d_{in}\,(U_i + c_{p_{CO_2}}\, J_{CO_2} + c_{p_{H_2}}\, J_{H_2})\,\Delta T \qquad (12)$$

The boundary conditions of above differential equations are listed as follows:

At $z = 0$:

$T_f = 140^{\circ}\text{C},\ n_{f,CO} = x_{CO} n_{t0},\ n_{f,H_2O} = x_{H_2O} n_{t0}$,

$n_{f,H_2} = x_{H_2} n_{t0}$, $n_{f,CO_2} = x_{CO_2} n_{t0}$

At $z = L$:

$T_s = 140^{\circ}\text{C}$, $n_{s,CO} = 0$, $n_{s,H_2O} = 0$,

$n_{s,H_2} = 5\times10^{-7}\ n_{t0}\ \gamma$, $n_{s,CO_2} = 370\times10^{-6} n_{t0}\ \gamma$

where n_{t0} is the feed molar flow rate, x is the molar fraction of the individual gas species in the gas mixture, and γ is the inlet sweep-to-feed molar flow rate ratio or sweep-to-feed ratio in the following paragraphs.

Although pure hydrogen is a superior fuel-cell fuel, currently there are issues on its storage and distribution [25]. As a more practical way, hydrogen used in an automotive fuel cell is suggested to be produced by reforming reactions of the available fuels, such as methanol, natural gas, gasoline and diesel. Steam reforming (SR), partial oxidation (POX) and autothermal reforming (ATR) are three major reforming processes. In SR, steam reacts with hydrocarbon over a catalyst to form H_2, CO and CO_2 at around 750 – 800°C since this reaction is strongly endothermic. In POX, the hydrocarbon reacts with a deficient amount of oxygen or air to produce H_2, CO and CO_2 while a large amount of heat is generated. ATR integrates these two processes together by feeding the hydrocarbon, water, and air together into the reactor at the same time. The SR reaction absorbs most of the heat generated by the POX reaction, and an overall process takes place slightly exothermally.

In this work, n_{t0} was 1 mol/s and 0.635 mol/s for autothermal reforming syngas and steam reforming syngas, respectively. With the compositions of both syngases given in Table 1, these flow rates were chosen because a sufficient H_2 molar flow rate would hence be provided to generate a power of 50 kW via the fuel cell for a five-passenger car [25]. Heated air was used as the sweep gas. The concentrations of hydrogen and carbon dioxide in the inlet air were set as 0.5 ppm and 370 ppm, respectively.

Table 1. The compositions of autothermal reforming syngas and steam reforming syngas.

	CO	H_2O	H_2	CO_2	N_2	CH_4
Autothermal reforming	1%	9.5%	41%	15%	33.5%	0%
Steam reforming	1%	18.2%	65.1%	15.5%	0%	0.2%

The bvp4c solver in Matlab® was used to solve the above differential equations of the boundary value problem with the given boundary conditions. During the calculation, the hollow fiber number was adjusted to satisfy the constraint of feed exit CO concentration, i.e., <10 ppm.

Autothermal Reforming Syngas

Reference Case

A reference case for the autothermal reforming synthesis gas was chosen with the CO_2/H_2 selectivity of 40, the CO_2 permeability of 4000 Barrers (1 Barrer = 10^{-10} cm^3 (STP) • cm/cm^2 • s • cm Hg), the inlet sweep-to-feed molar flow rate ratio of 1, the membrane thickness of 5 μm, 52,500 hollow fibers (a length of 61 cm, an inner diameter of 0.1 cm, and a porous support with a porosity of 50% and a thickness of 30 μm), both inlet feed and sweep temperatures of 140°C, and the feed and sweep pressures of 3 and 1 atm, respectively. With respect to this case, the effects of CO_2/H_2 selectivity, CO_2 permeability, sweep-to-feed ratio, inlet feed temperature, inlet sweep temperature, feed pressure, and catalyst acitivity on the reactor behavior were then investigated.

Figure 7 shows the profiles of the feed-side mole fractions of CO and CO_2 along the length of the countercurrent membrane reactor. The modeling results demonstrated that this membrane reactor could decrease CO concentration from 1% to 9.82 ppm along with the removal of almost all the CO_2.

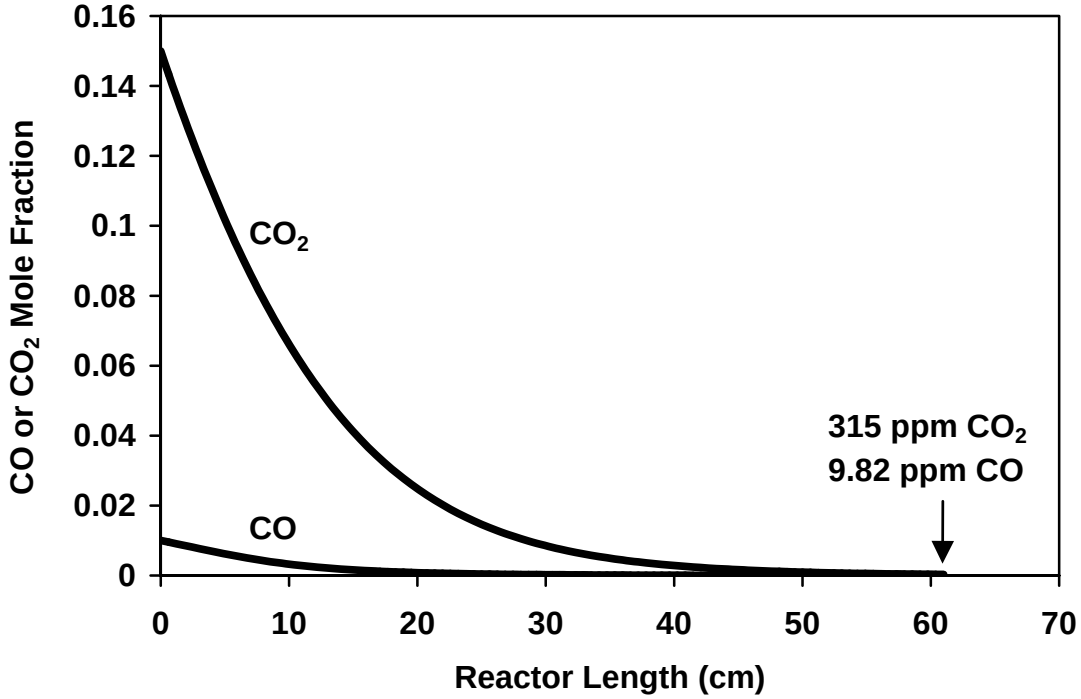

Figure 7. Feed-side CO and CO_2 mole fraction profiles along the length of membrane reactor for autothermal reforming syngas.

Figure 8 depicts the profiles of feed-side H_2 concentrations on the dry and wet bases. As depicted in this figure, the membrane reactor could enhance H_2 concentration from 45.30% to 54.95% (on the dry basis), i.e., from 41% to 49.32% (on the wet basis). In this case, the H_2 recovery calculated from the model was 97.38%. With the advancement of the high temperature proton-exchange-membrane fuel cell (120 – 160°C), it is expected that the constraint of CO concentration can be relaxed to about 50 ppm in the near future. Then, the required hollow fiber number could be reduced significantly to 39,000 based on the modeling results.

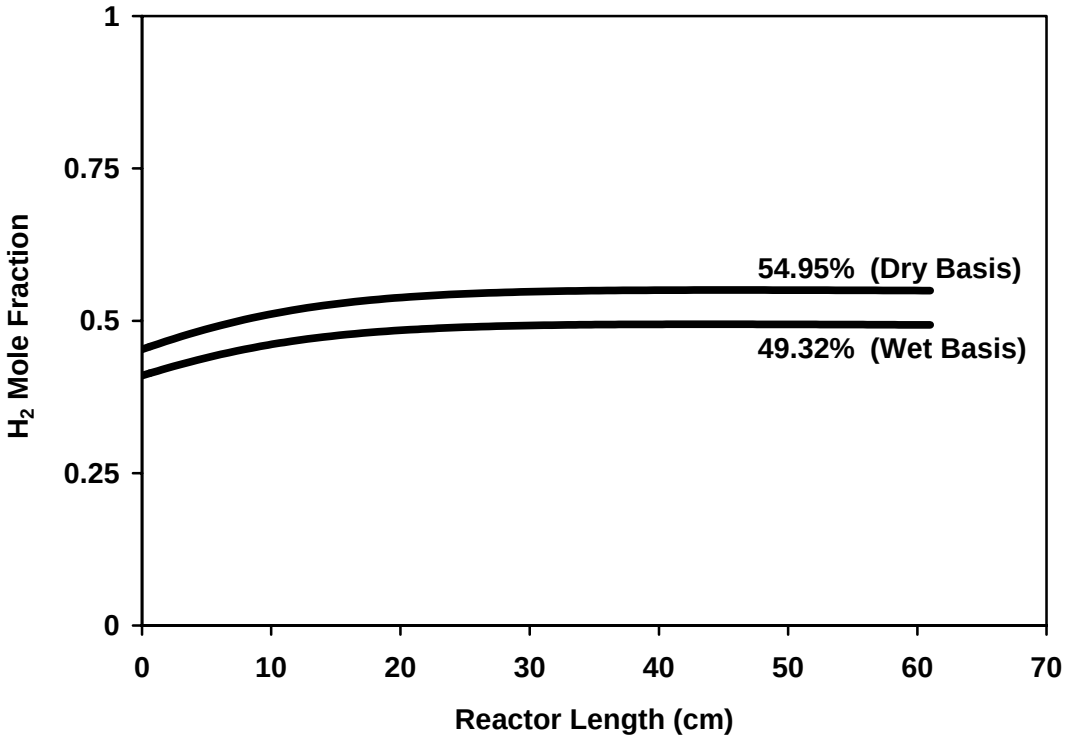

Figure 8. Feed-side H_2 mole fraction profiles along the length of membrane reactor for autothermal reforming syngas.

The temperature profiles for both feed and sweep sides are shown in Figure 9 with a maximum for each profile. Since the overall module was adiabatic, the feed gas was heated by the exothermic WGS reaction. The highest feed-side temperature was 158°C at about z = 15 cm. Beyond that, the feed-side temperature reduced, and it became very close to the sweep-side temperature at the end of membrane reactor. This was due to the efficient heat transfer provided by the hollow fiber configuration. Higher temperatures enhance WGS reaction rates but are unfavorable for CO conversion. Thus, it is important to use air with appropriate temperature, i.e., 140°C as the sweep gas to keep the feed gas within 150 ± 10°C.

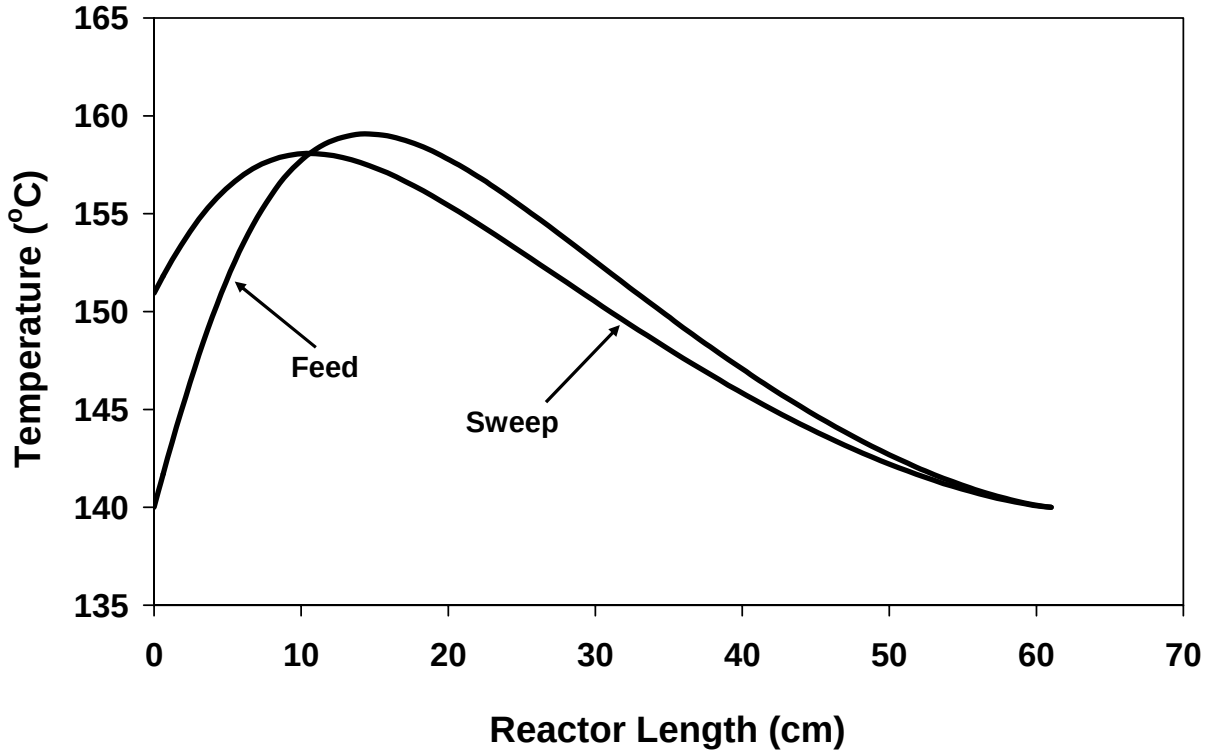

Figure 9. Feed-side and sweep-side temperature profiles along the length of membrane reactor for autothermal reforming syngas.

Effect of CO_2/H_2 Selectivity

In order to study the impact of CO_2/H_2 selectivity on the membrane reactor performance, α = 10, 20, 40, 60 and 80 were applied in the model while the other parameters for the reference case were kept constant. As shown in Figure 10, the feed-side exit CO concentration increased slightly as the CO_2/H_2 selectivity increased. This was due to the fact that higher selectivity caused lower H_2 permeability and thus a lower H_2 permeation rate or higher H_2 concentration on the feed side, which was unfavorable for the WGS reaction rate. Also shown in this figure, the H_2 recovery increased from 89.85% to 98.68% as the CO_2/H_2 selectivity increased from 10 to 80. This indicated that the higher selectivity decreased the H_2 loss because of the reduction in H_2 permeation through the membrane. In addition, the modeling results showed that a CO_2/H_2 selectivity of 10 was the minimum value required for a H_2 recovery of about 90%.

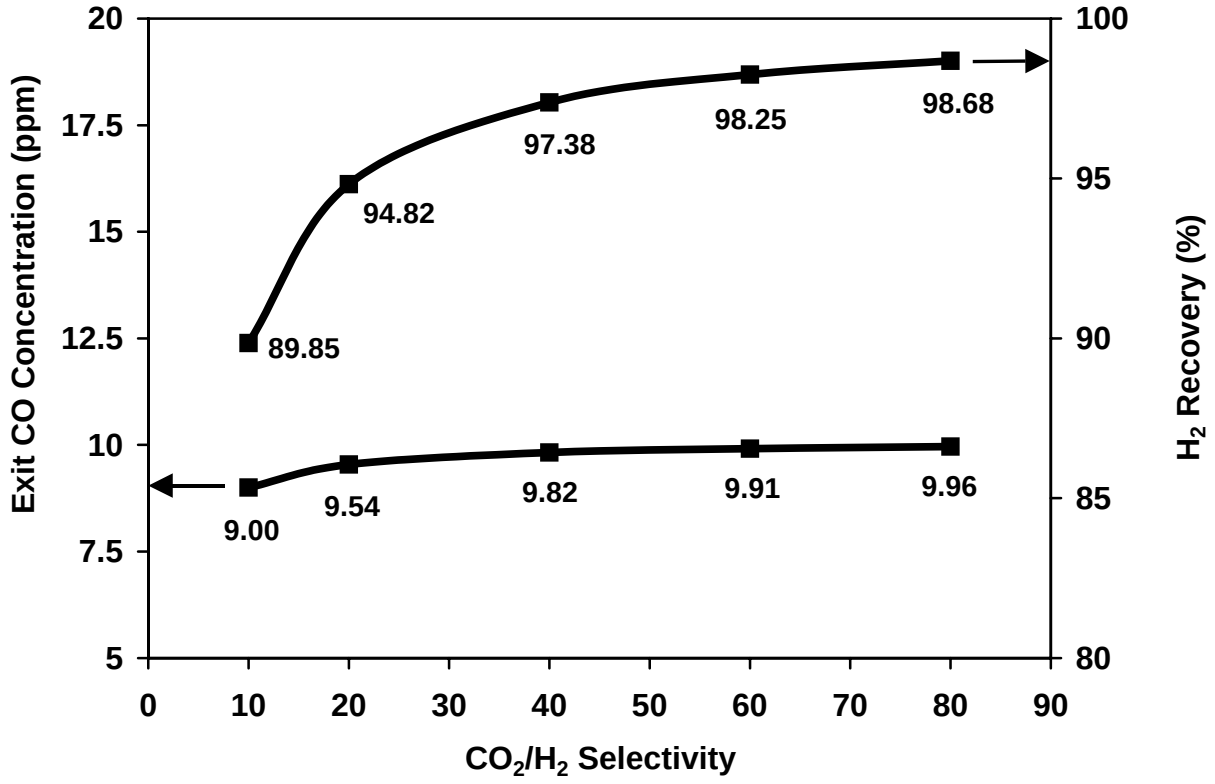

Figure 10. The effects of CO_2/H_2 selectivity on feed-side exit CO concentration and H_2 recovery for autothermal reforming syngas.

Effect of CO_2 Permeability

The membrane areas required for the exit feed CO concentration of <10 ppm in the H_2 product were calculated with five different CO_2 permeabilities ranging from 1000 to 8000 Barrers while the other parameters for the reference case were kept constant. As demonstrated in Figure 11, the required membrane area or hollow fiber number dropped rapidly as permeability increased from 1000 Barrers to 4000 Barrers. Beyond that, it approached an asymptotic value gradually. Increasing CO_2 permeability increased the CO_2 permeation rate and enhanced the CO_2 removal, which shifted the WGS reaction towards the product side. However, after the permeability exceeded about 6000 Barrers, the overall system became reaction controlled. Hence, the influence of the permeability became less significant.

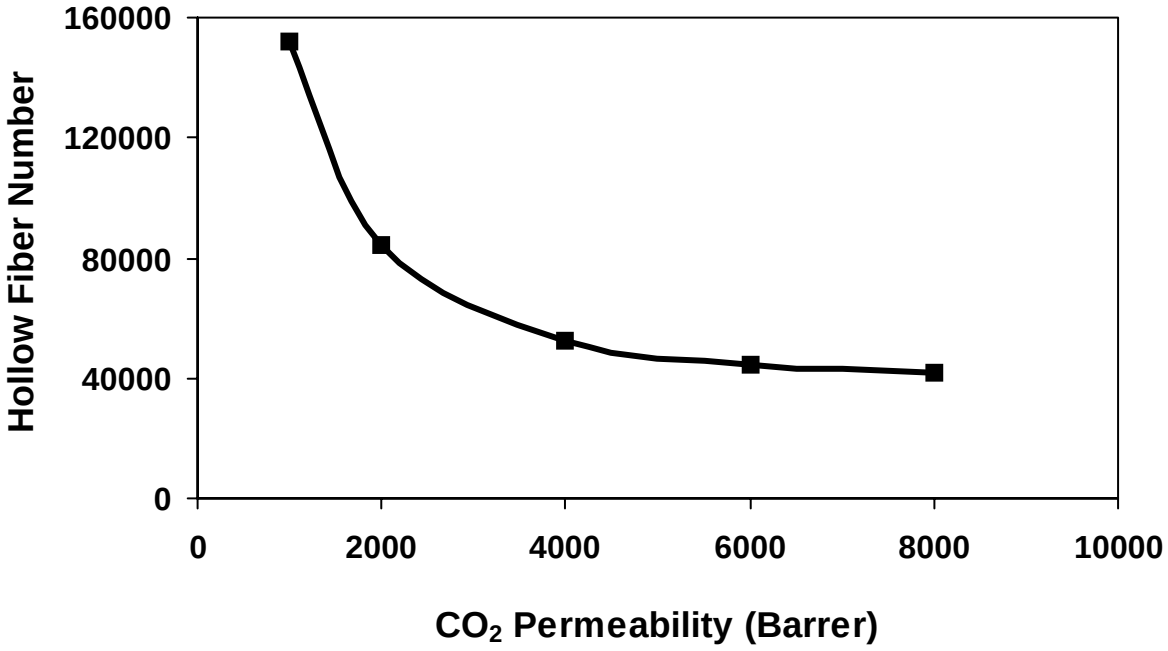

Figure 11. The effect of CO_2 permeability on required membrane area for autothermal reforming syngas.

Effect of Sweep-to-Feed Ratio

The inlet sweep-to-feed molar flow rate ratios of 0.5, 1, 1.5, 2 and 2.5 were used in the calculation while the other parameters for the reference case were kept constant. Figure 12 illustrates the effect of sweep-to-feed ratio on feed-side exit CO concentration. As illustrated in this figure, increasing the sweep-to-feed ratio decreased the exit CO concentration first and then increased it slightly. A higher sweep-to-feed ratio resulted in a lower CO_2 concentration on the sweep side and then a higher CO_2 permeation driving force. However, it also enhanced heat transfer and then decreased the feed-side temperature, which was unfavorable to the WGS reaction rate. Therefore, an optimal sweep-to-feed ratio of about 1 existed as a result of the tradeoff between the effects on the CO_2 permeation rate and the WGS reaction rate. Also illustrated in this figure is the effect of sweep-to-feed ratio on H_2 recovery. The sweep-to-feed ratio did not have a significant effect on the H_2 recovery. This was due to the fact that the resulting CO concentrations were very low (<30 ppm) and did not affect the H_2 recovery.

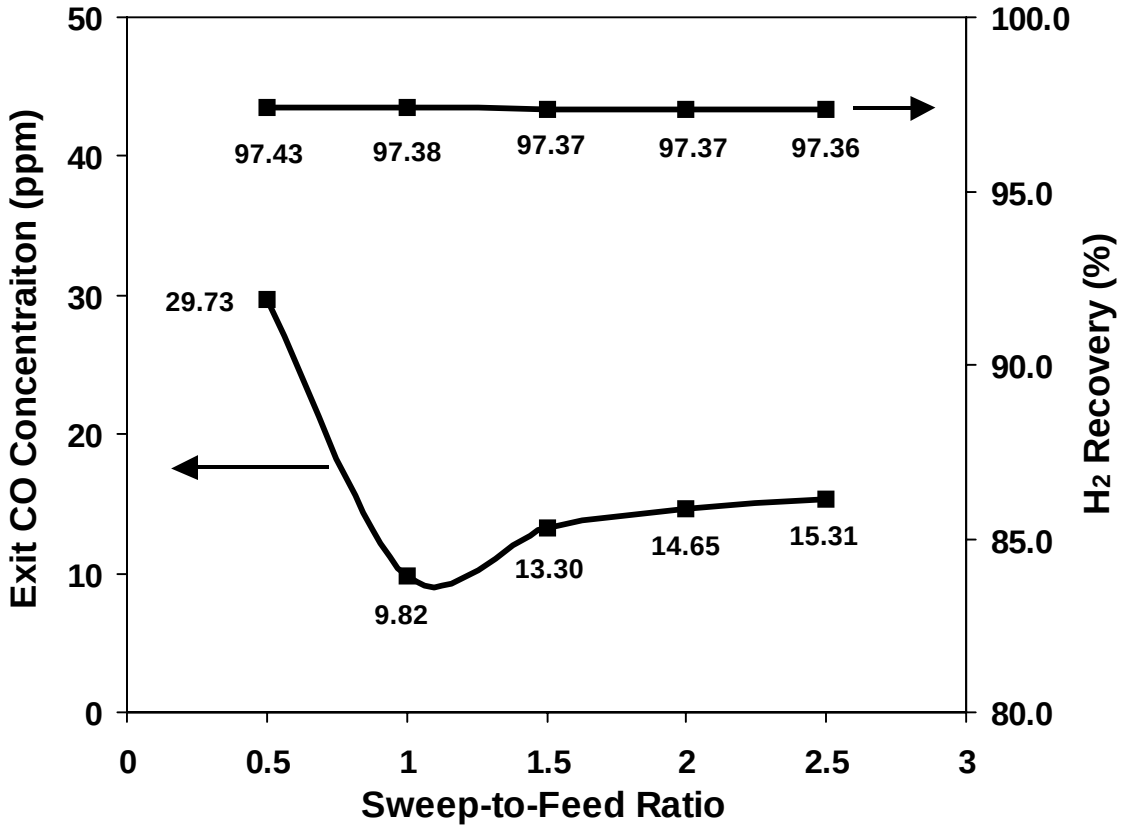

Figure 12. The effects of sweep-to-feed ratio on feed-side exit CO concentration and H_2 recovery for autothermal reforming syngas.

Effect of Inlet Feed Temperature

In order to study the impact of inlet feed temperature on the membrane reactor performance, T_{f0} = 80, 100, 120, 140, 160, 180 and 200^{o}C were applied in the model while the other parameters for the reference case were kept constant. As shown in Figure 13, the required membrane area or hollow fiber number decreased as the inlet feed temperature increased. It approached an asymptotic value gradually. The feed side temperature profiles for different feed inlet temperatures are presented in Figure 14. The feed side temperature increased as the inlet feed temperature increased especially at the entrance section. The higher feed side temperature gave a higher WGS reaction rate, and thus a less reactor or catalyst volume, i.e., a lower membrane area, was required. The unfavorable WGS equilibrium at high temperatures was compensated by the simultaneous CO_2 removal.

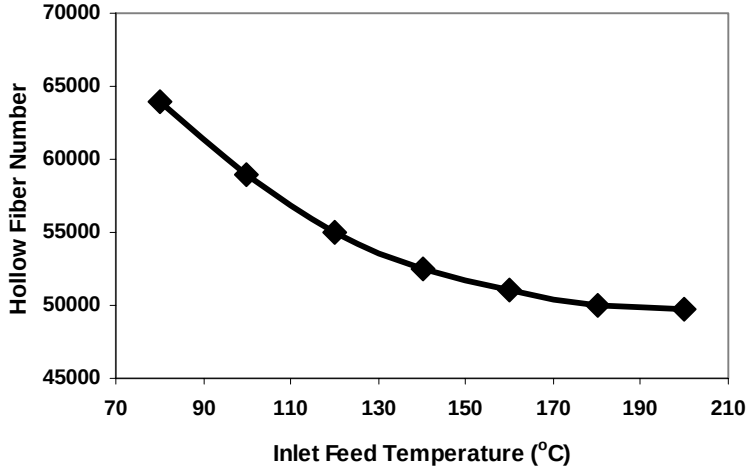

Figure 13. The effect of inlet feed temperature on required membrane area for autothermal reforming syngas.

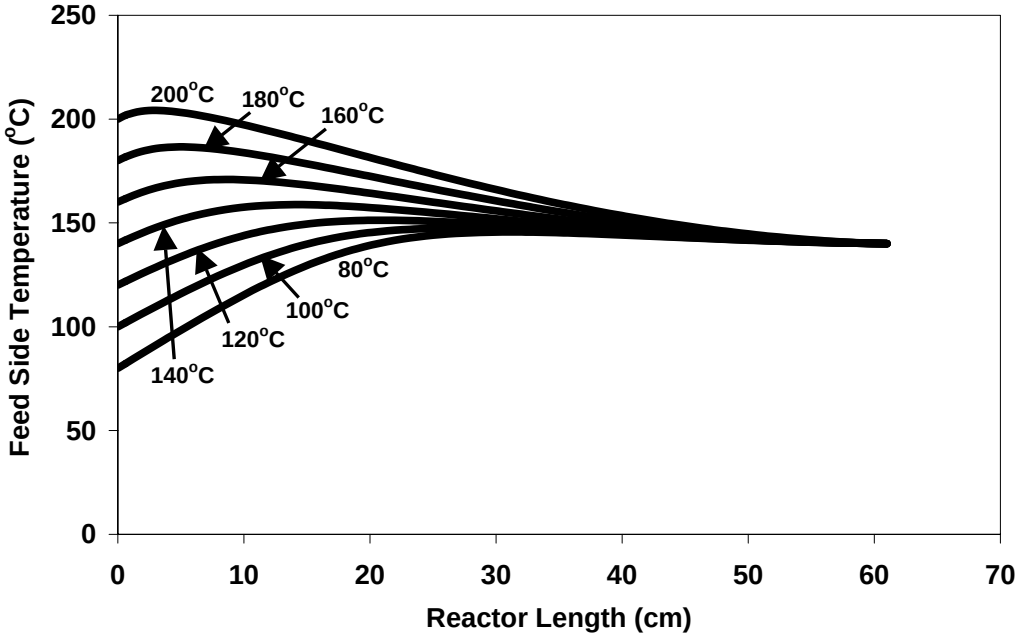

Figure 14. Feed-side temperature profiles along the length of membrane reactor for autothermal reforming syngas with different inlet feed temperatures.

Effect of Inlet Sweep Temperature

The membrane areas required for the exit feed CO concentration of <10 ppm in the H_2 product were calculated with seven different inlet sweep temperatures ranging from 80 to 200°C, while the other parameters for the reference case were kept constant. As demonstrated in Figure 15, the required membrane area or hollow fiber number dropped rapidly as the inlet sweep temperature increased from 80°C to 160°C. Beyond 160°C, it increased slightly. Figure 16 depicts the feed side temperature profiles along the membrane reactor with different inlet sweep

temperatures. Increasing the inlet sweep temperature increased the feed side temperature significantly over a longer reactor length in comparison with increasing the inlet feed temperature as shown in Figure 14. A higher feed side temperature resulted in a higher WGS reaction rate and thus a lower membrane area as described earlier. When the inlet sweep temperature exceeded about 160°C, the WGS reaction equilibrium became less favorable, and the overall system became more mass transfer controlled. Hence, more membrane area was needed to remove the generated CO_2 to achieve < 10 ppm CO in the H_2 product.

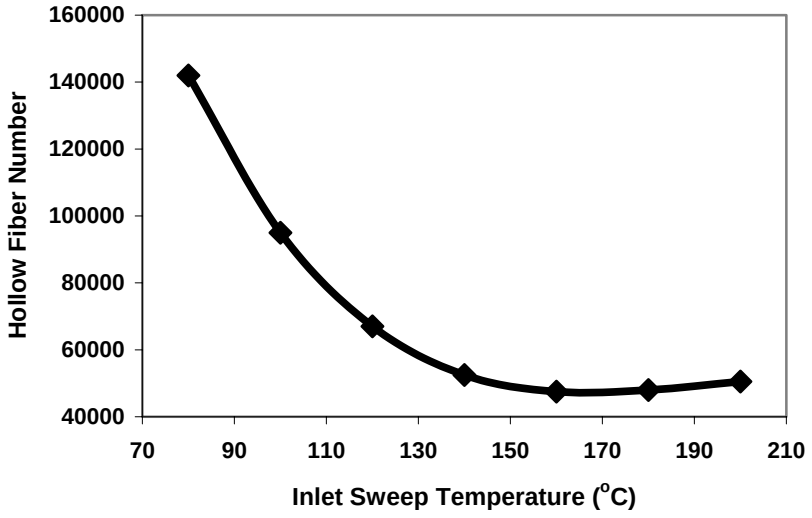

Figure 15. The effect of inlet sweep temperature on required membrane area for autothermal reforming syngas.

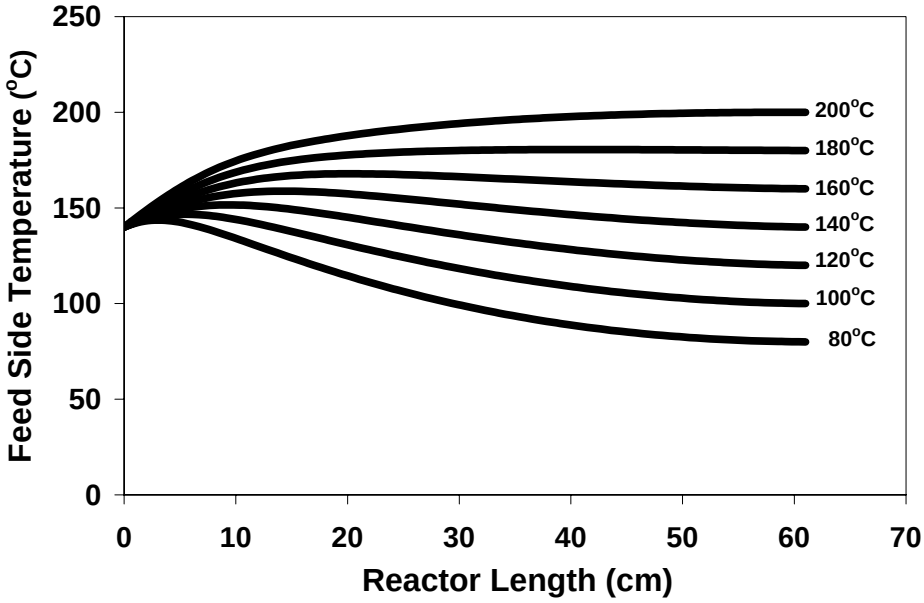

Figure 16. Feed-side temperature profiles along the length of membrane reactor for autothermal reforming syngas with different inlet sweep temperatures.

Effect of Feed Pressure

Five different feed pressures ranging from 2 to 6 atm were used in the calculation while other parameters for the reference case were kept constant. The effect of feed pressure on the required membrane area for the exit feed CO concentration of <10 ppm is depicted in Figure 17. As depicted in this figure, increasing feed pressure decreased the required membrane area significantly, particularly from 2 to 4 atm. The higher feed pressure gave a higher CO_2 partial pressure on the feed side and thus a greater CO_2 permeation rate. This resulted in the reduced membrane area.

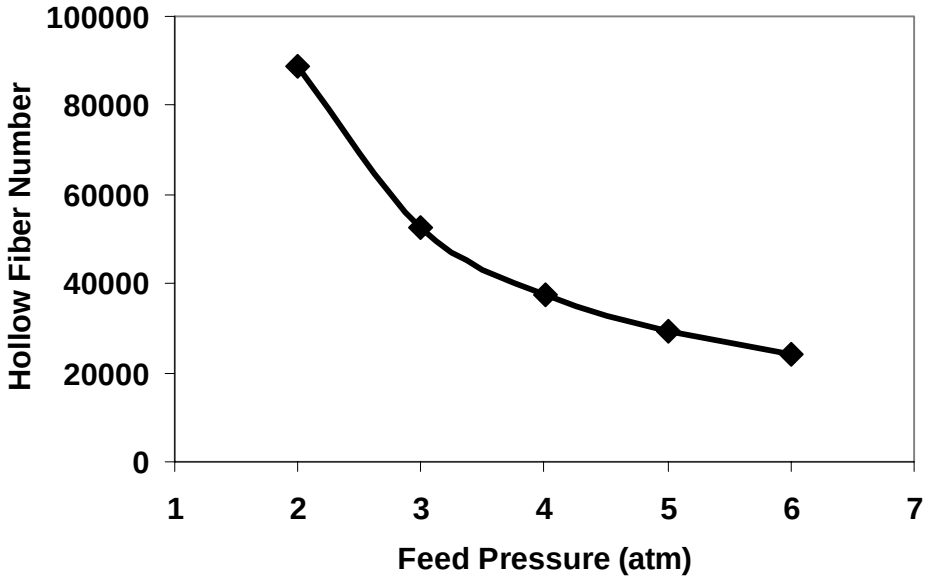

Figure 17. The effect of feed pressure on required membrane area for autothermal reforming syngas.

Effect of Catalyst Activity

The effect of catalyst activity on the required membrane area was studied by assuming several WGS reaction kinetics based on the Cu/ZnO kinetics equation proposed by Keiski et al. [14]. In Figure 18, the number on the horizontal x axis indicates the reaction kinetic rate in terms of the times of the Cu/ZnO kinetics, e.g., 1 represents the Cu/ZnO kinetics, 2 represents a kinetics of 2 times the Cu/ZnO kinetics, etc. As illustrated in this figure, increasing catalyst activity reduced the required membrane area significantly. The higher catalyst activity resulted in a higher reaction rate, which also increased the CO_2 permeation rate because of a higher CO_2 partial pressure on the feed side and thus a higher driving force across the membrane. Hence, with the advancement of a more active WGS catalyst, the membrane reactor would become more compact.

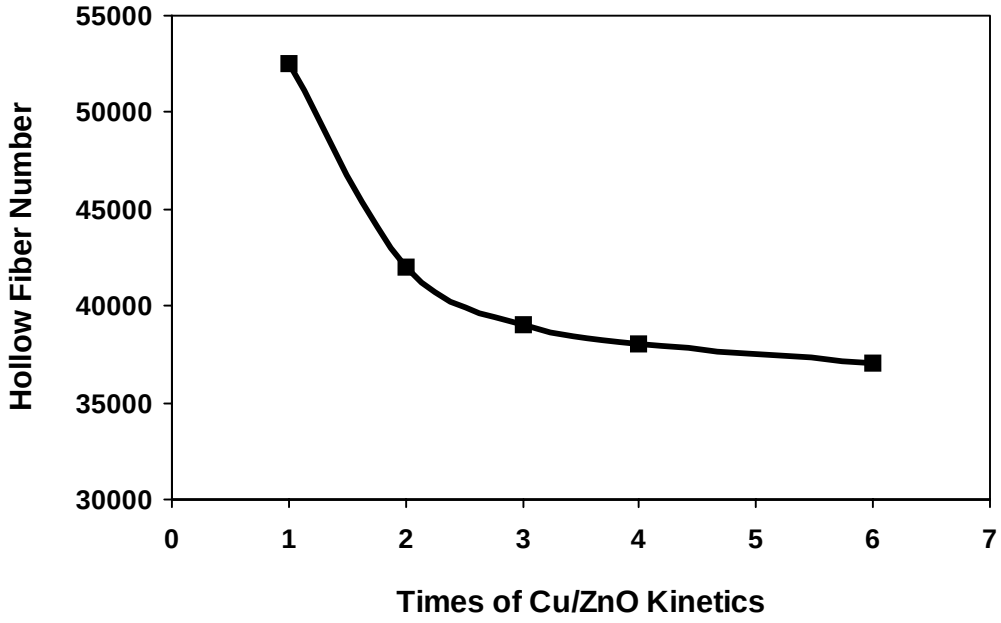

Figure 18. The effect of catalyst activity on required membrane area for autothermal reforming syngas.

Steam Reforming Syngas

Reference Case

For the steam reforming syngas, we chose a reference case with the same system parameter values as those for the autothermal reforming syngas except 31,000 hollow fibers with the same dimensions described earlier. The reduced number of hollow fibers for the steam reforming syngas was due to the fact that this syngas had a higher H_2 concentration and thus a lower flow rate than autothermal reforming syngas. Similarly, the effects of CO_2/H_2 selectivity, CO_2 permeability, sweep-to-feed ratio, inlet feed temperature, inlet sweep temperature, feed pressure, and catalyst acitivity on the reactor behavior were investigated for the steam reforming syngas with respect to the reference case.

Figure 19 shows the profiles of the feed-side mole fractions of CO and CO_2 along the length of the membrane reactors. The modeling results showed that this membrane reactor could decrease CO concentration from 1% to 9.89 ppm along with the removal of almost all the CO_2.

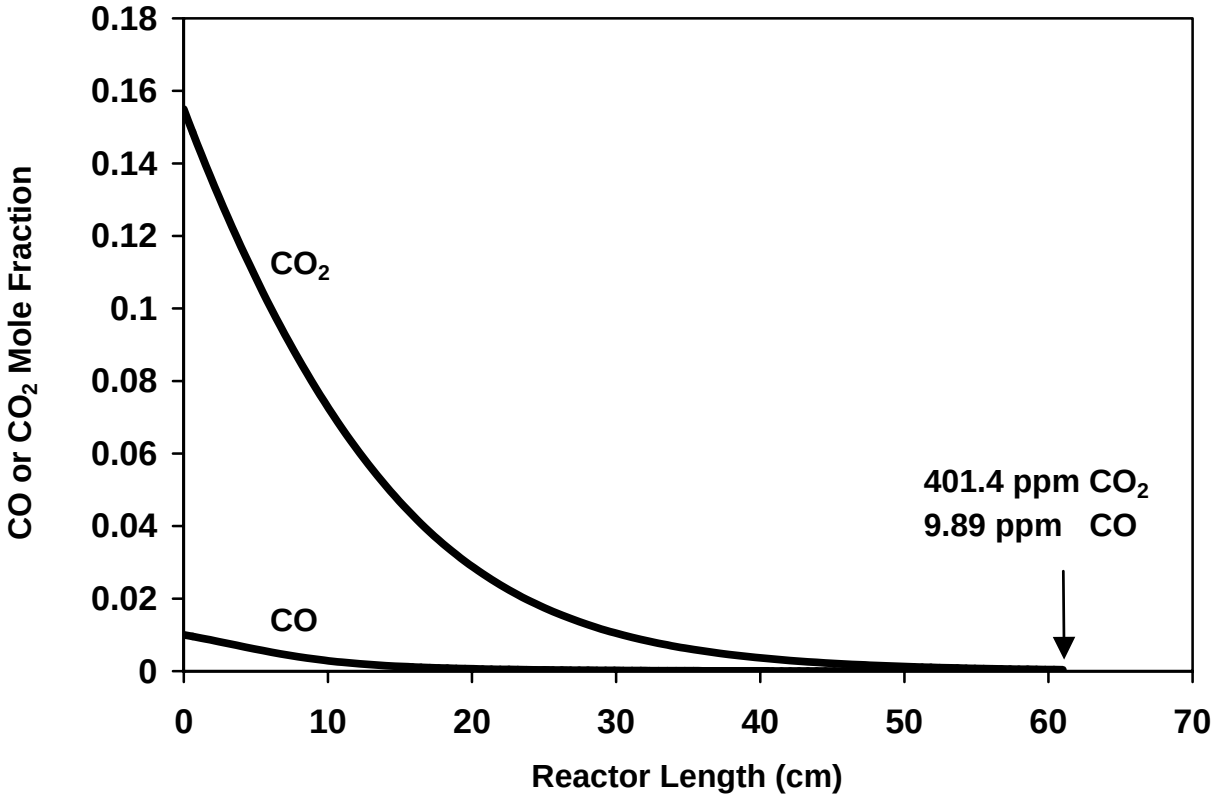

Figure 19. Feed-side CO and CO_2 mole fraction profiles along the length of membrane reactor for steam reforming syngas.

Figure 20 depicts the profiles of feed-side H_2 concentrations on the dry and wet bases. As depicted in this figure, the membrane reactor could enhance H_2 concentration from 79.58% to 99.64% (on the dry basis with the balance of the H_2 product, i.e., 0.36%, being methane mainly) or from 65.1% to 78.69% (on the wet basis). In this case, H_2 recovery was 97.38%. Compared with the outlet gas from the autothermal reforming syngas, a much higher exit H_2 concentration was obtained from the steam reforming syngas. This was attributed to the higher inlet H_2 concentration and no N_2 in the steam reforming syngas. Higher hydrogen concentration is believed to improve fuel cell performance. However, since the steam reforming reaction is strongly endothermic, a large and heavy reactor is needed to meet the heat exchange requirement. With smaller and lighter hardware, the autothermal reforming process is generally considered to be more attractive for on-broad hydrogen generation for the automotive fuel cell system [26].

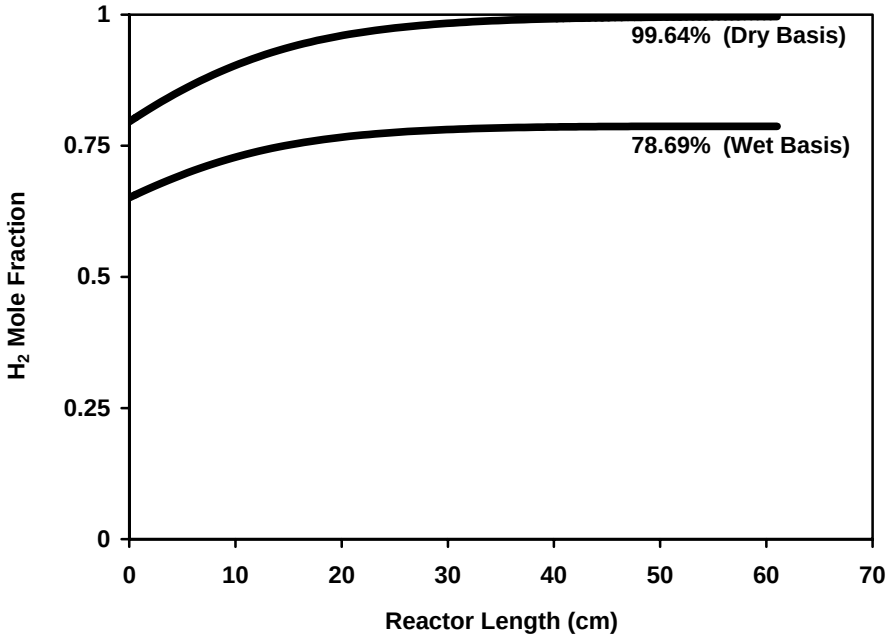

Figure 20. Feed-side H_2 mole fraction profiles along the length of membrane reactor for steam reforming syngas.

The temperature profiles for both feed and sweep sides are illustrated in Figure 21. As illustrated in this figure, maximum temperatures existed for both feed and sweep sides due to the heat of the WGS reaction generated in the adiabatic module, as explained earlier for the autothermal reforming syngas.

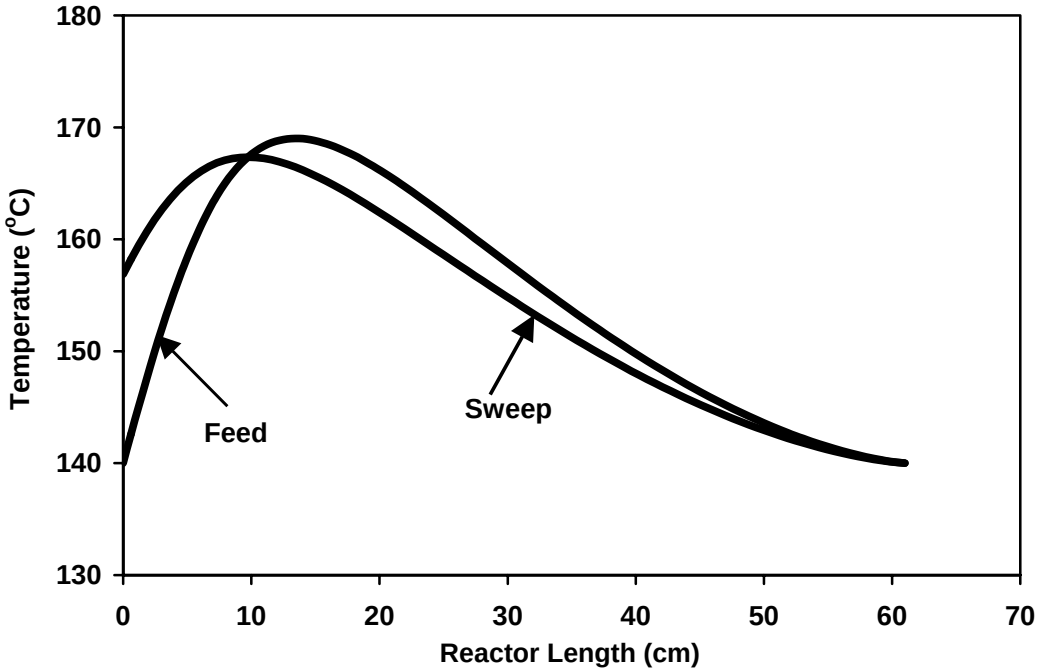

Figure 21. Feed-side and sweep-side temperature profiles along the length of membrane reactor for steam reforming syngas.

Effect of CO_2/H_2 Selectivity

The CO_2/H_2 selectivity values of 10, 20, 40, 60 and 80 were applied in the model to study the selectivity impact on the membrane reactor performance while the other parameters for the reference case were kept constant. As shown in Figure 22, the curves for feed-side exit CO concentration and H_2 recovery showed consistent trends with those for the autothermal reforming syngas in Figure 10. Both exit CO concentration and H_2 recovery increased as the CO_2/H_2 selectivity increased. As explained earlier, the lower H_2 permeation rate from higher selectivity increased the exit CO concentration and the H_2 recovery.

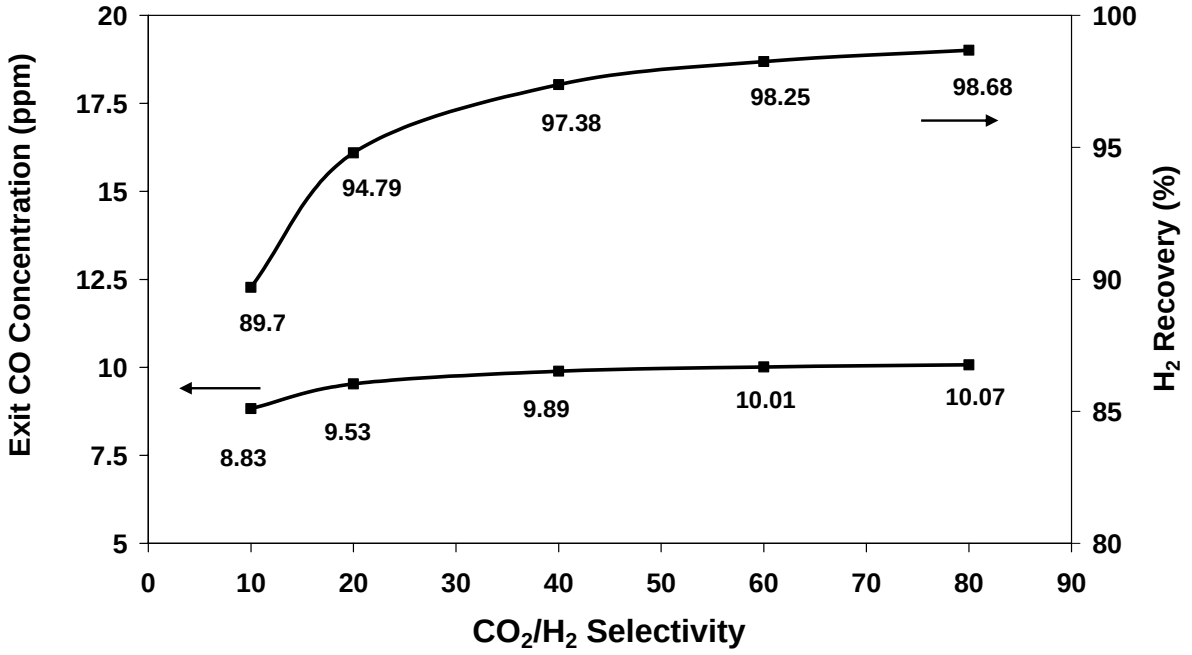

Figure 22. The effects of CO_2/H_2 selectivity on feed-side exit CO concentration and H_2 recovery for steam reforming syngas.

Effect of CO_2 Permeability

Five different CO_2 permeabilities ranging from 1000 to 8000 Barrers were used in the calculation while other parameters for the reference case were kept constant. The effect of CO_2 permeability on the required membrane area for the exit feed CO concentration of <10 ppm is presented in Figure 23. Similar to the autothermal reforming syngas, the required hollow fiber number decreased significantly as CO_2 permeability increased. Higher CO_2 permeability enhanced the CO_2 permeation, which shifted the WGS reaction towards the product side. Therefore, the required membrane area or hollow fiber number was reduced.

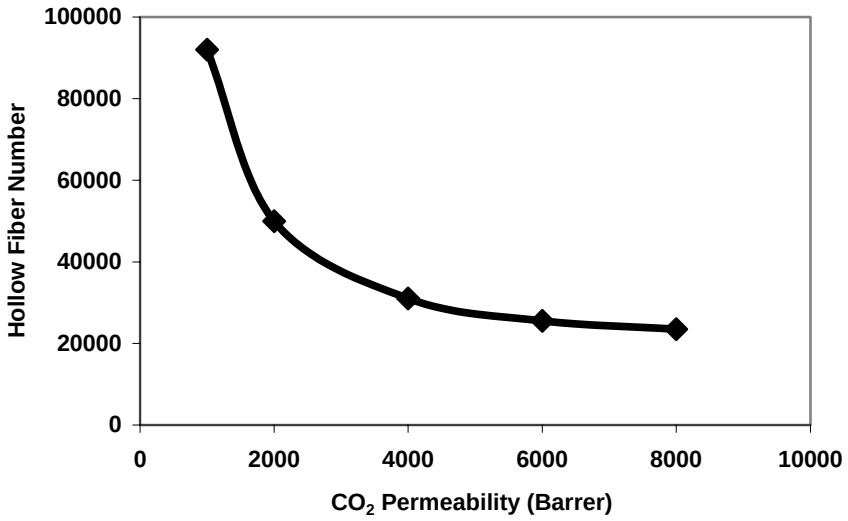

Figure 23. The effect of CO_2 permeability on required membrane area for steam reforming syngas.

Effect of Sweep-to-Feed Ratio

The inlet sweep-to-feed molar flow rate ratios of 0.5, 1, 1.5, 2 and 2.5 were used in the calculation while the other parameters for the reference case were kept constant. Figure 24 illustrates the effect of sweep-to-feed ratio on feed-side exit CO concentration and H_2 recovery. Similar to the autothermal reforming syngas, the exit CO concentration decreased and then increased as the sweep-to-feed ratio increased. A minimum CO value existed at the sweep-to-feed ratio of about 1. A higher sweep-to-feed ratio enhanced the CO_2 permeation but also decreased the feed side temperature. The balance between the two opposite effects resulted in the lowest exit CO concentration. H_2 recovery did not change significantly with different sweep-to-feed ratios, due to the reason explained earlier.

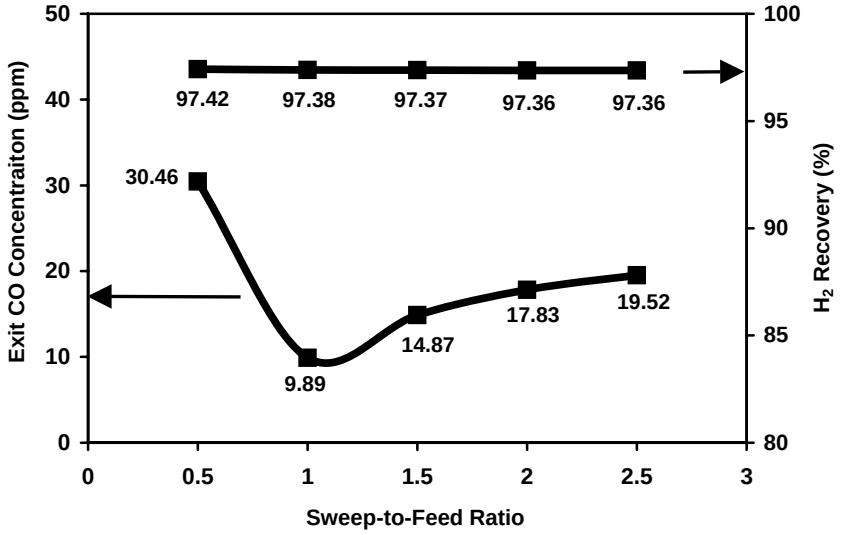

Figure 24. The effects of sweep-to-feed ratio on feed-side exit CO concentration and H_2 recovery for steam reforming syngas.

Effect of Inlet Feed Temperature

The inlet feed temperatures of 80, 100, 120, 140, 160, 180 and 200^{o}C were applied in the model to study the impact of inlet feed temperature on the membrane reactor performance while the other parameters for the reference case were kept constant. As demonstrated in Figure 25, the curves for the required membrane area showed consistent trends with those for the autothermal reforming syngas. The required membrane area decreased as the feed inlet temperature increased. Figure 26 shows the feed side temperature profiles for different inlet feed temperatures. As explained earlier, the higher feed side temperature from the higher inlet feed temperature increased the WGS reaction rate and decreased the membrane area requirement.

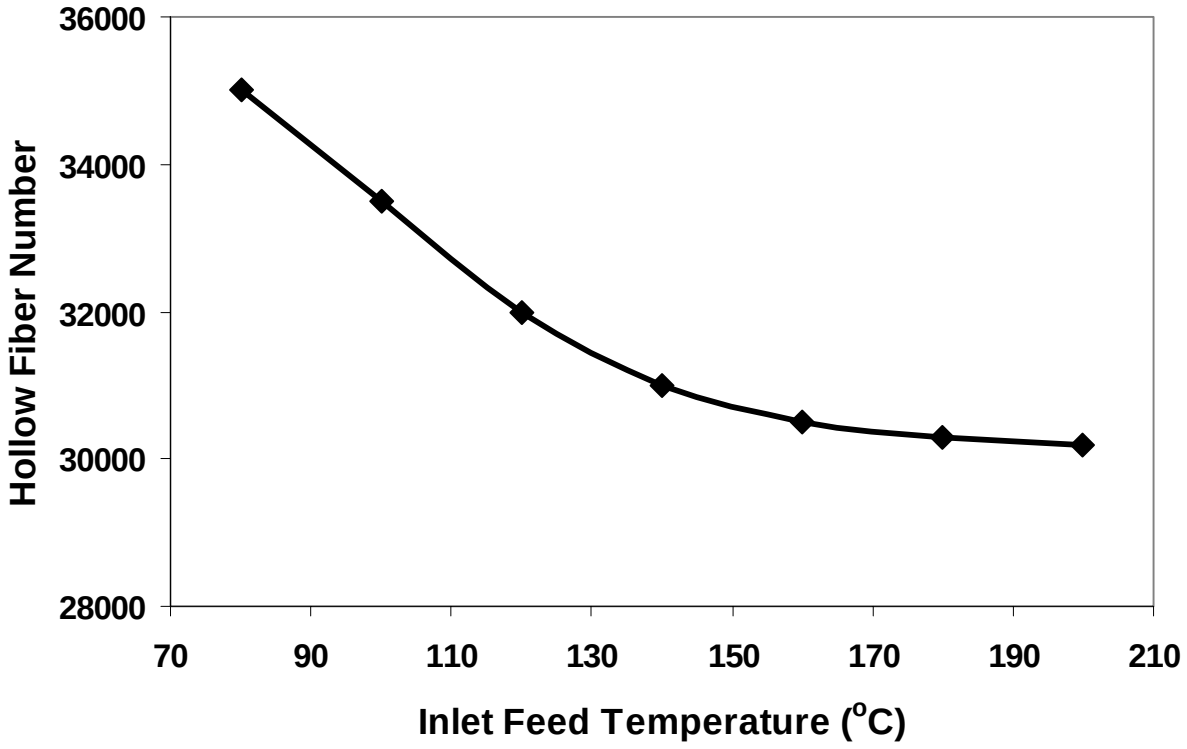

Figure 25. The effect of inlet feed temperature on required membrane area for steam reforming syngas.

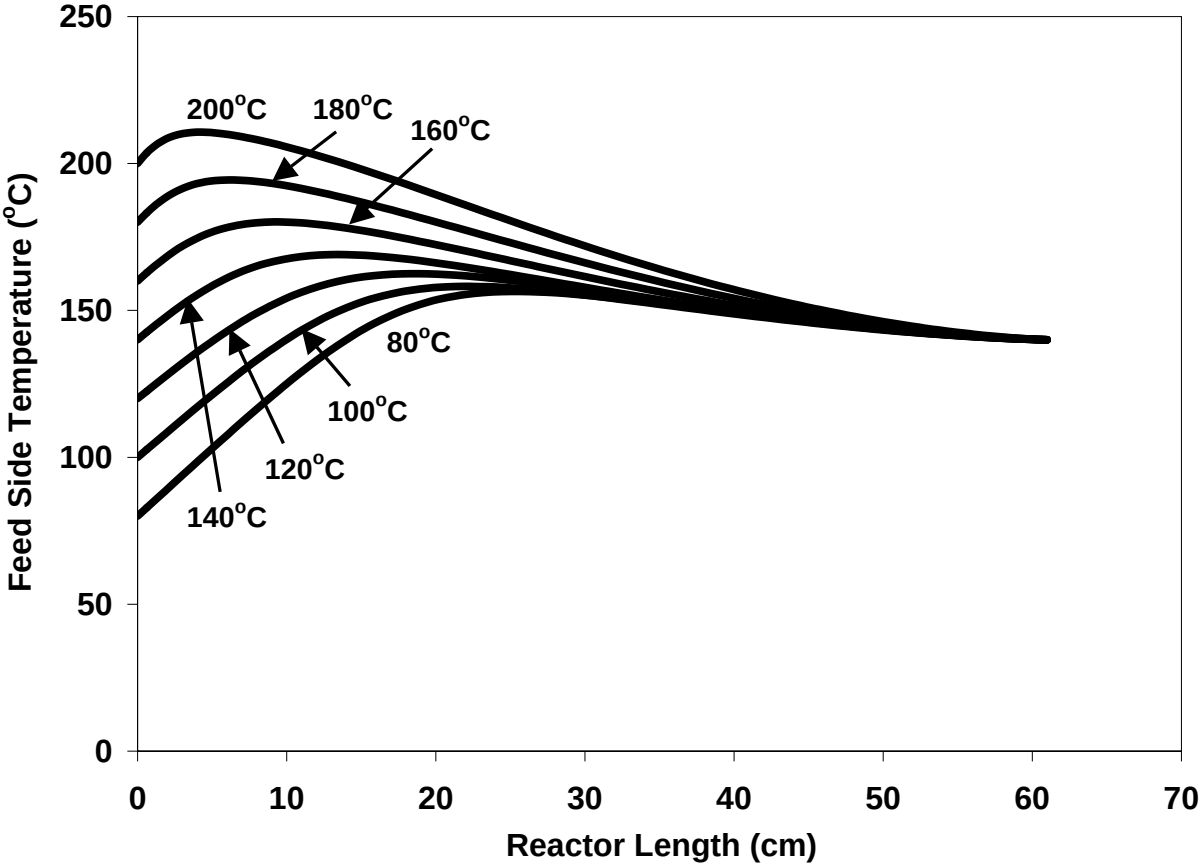

Figure 26. Feed-side temperature profiles along the length of membrane reactor for steam reforming syngas with different inlet feed temperatures.

Effect of Inlet Sweep Temperature

Seven different inlet sweep temperatures ranging from 80 to 200°C were used in the calculation while other parameters for the reference case were kept constant. The effect of inlet sweep temperature on the required membrane area for the exit feed CO concentration of <10 ppm is presented in Figure 27. Similar to the autothermal reforming syngas, the required hollow fiber number decreased significantly as the inlet sweep temperature increased, a minimal value existed at ~ 170°C. As shown in Figure 28, the higher inlet sweep temperatures increased the feed side temperatures significantly over the most of reactor length, which increased the WGS reaction rate. When the inlet sweep temperature exceeded about 170°C, the WGS reaction equilibrium became less favorable, and the overall system became more mass transfer controlled. Hence, more membrane area was needed to reduce the feed exit CO concentration to less than 10 ppm.

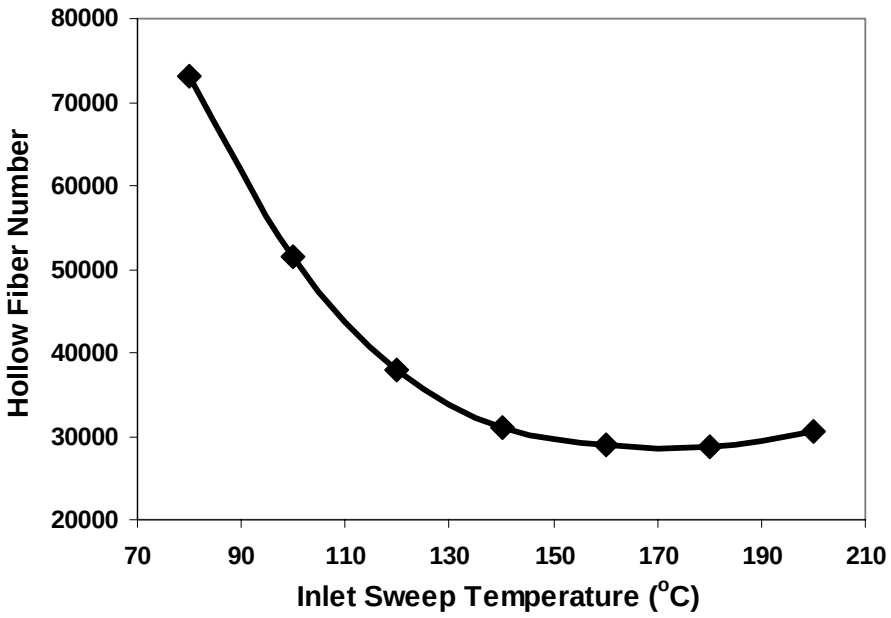

Figure 27. The effect of inlet sweep temperature on required membrane area for steam reforming syngas.

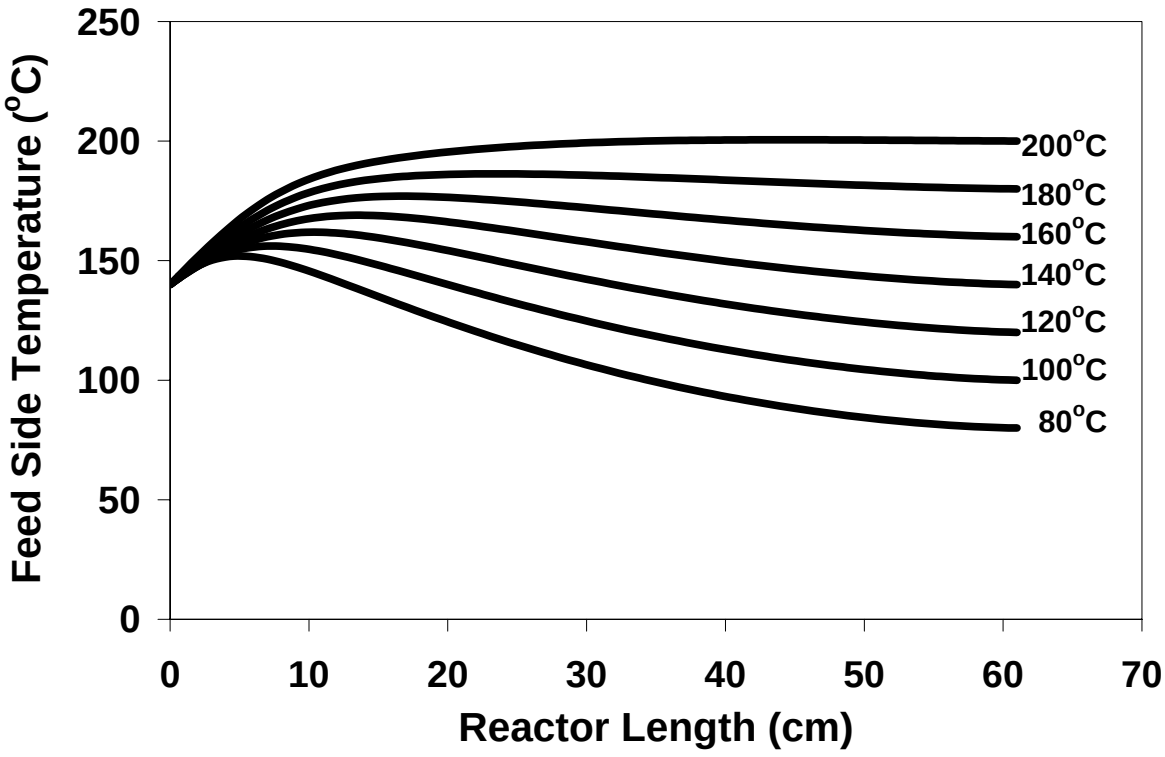

Figure 28. Feed-side temperature profiles along the length of membrane reactor for steam reforming syngas with different inlet sweep temperatures.

Effect of Feed Pressure

To investigate the effect of feed pressure on the required membrane area for <10 ppm CO in the H_2 product, five different feed pressures ranging from 2 to 6 atm were used in the calculation while other parameters for the reference case were kept constant. As shown in Figure 29, increasing feed pressure decreased the required membrane area significantly, particularly from 2 to 4 atm. This behavior was similar to that for the autothermal reforming syngas described earlier.

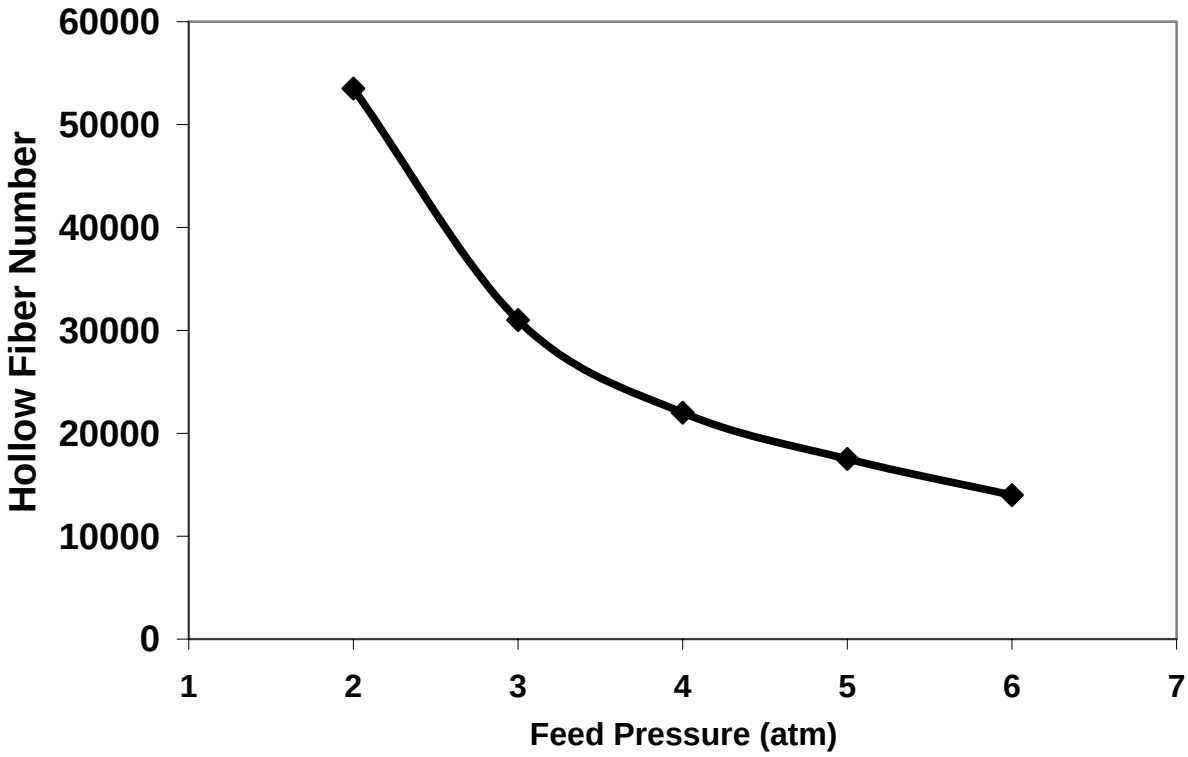

Figure 29. The effect of feed pressure on required membrane area for steam reforming syngas.

Effect of Catalyst Activity

Figure 30 illustrates the effect of catalyst activity on the required membrane area to satisfy the constraint of feed exit CO concentration. As illustrated in this figure, the membrane area required decreased significantly as the catalyst activity increased, which had a similar trend as the autothermal reforming syngas. As explained earlier, a higher catalyst activity increased the WGS reaction rate and enhanced the CO_2 permeation because of a higher driving force. Therefore, the higher catalyst activity resulted in a small amount of catalyst or a small reactor size.

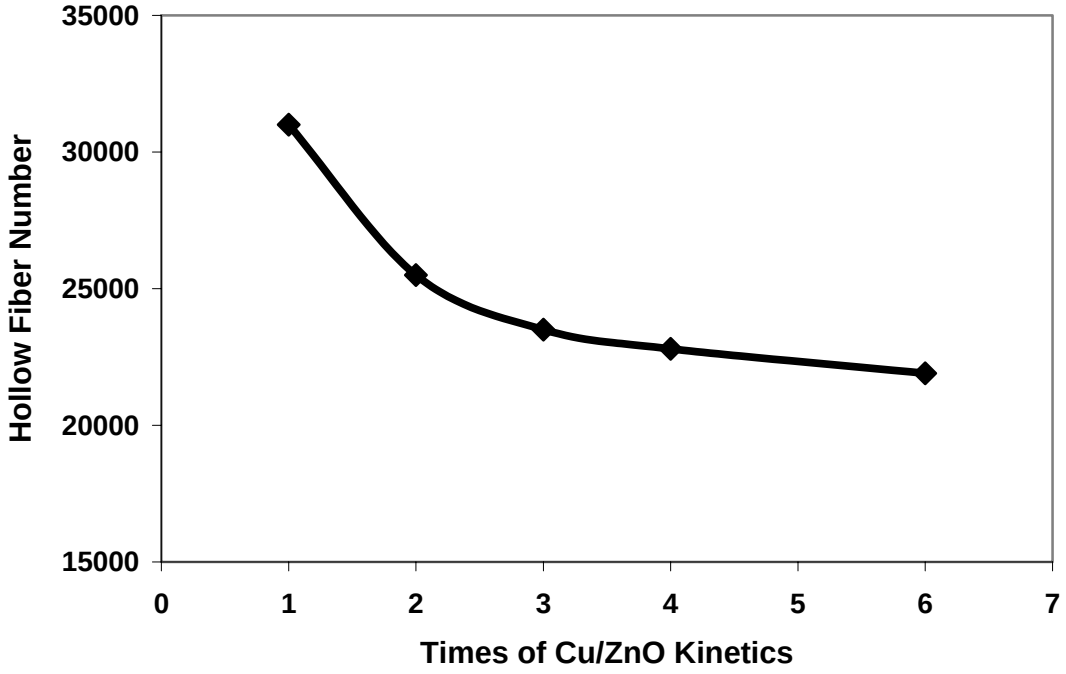

Figure 30. The effect of catalyst activity on required membrane area for steam reforming syngas.

Modeling of Membrane Reactor Using Membrane Data Obtained

We used the selectivity and flux data obtained as the input to the mathematical model developed [10-12] to show the feasibility of achieving H_2 enhancement, CO reduction to $\leq$ 10 ppm, and high H_2 recovery, to study the effects of system parameters on the reactor, and to guide / minimize experimental work. The CO_2/H_2 selectivity of 40 and the CO_2 permeability of 4000 Barrers were used again in the modeling work. We have investigated the performance of the countercurrent membrane reactor for the synthesis gases from the autothermal reforming of gasoline with air. The three synthesis gases investigated at 3 atm contained CO at concentrations of 10%, 5%, and 1%. Figure 31 illustrates the profiles of the CO concentration in the H_2 product for a total reactor length of 61 cm for these three feed CO concentrations. As shown in this figure, a H_2 product with less than 10 ppm CO was obtained from each of these synthesis gases. In the membrane reactor for each of these synthesis gases, the syngas flow with an inlet temperature of 140^{o}C was countercurrent to the flow of hot air sweep with an inlet temperature of 140^{o}C, the molar flow rate ratio of the air sweep to the syngas (γ) was 1, and the catalyst was the commercial Cu/ZnO supported on alumina.

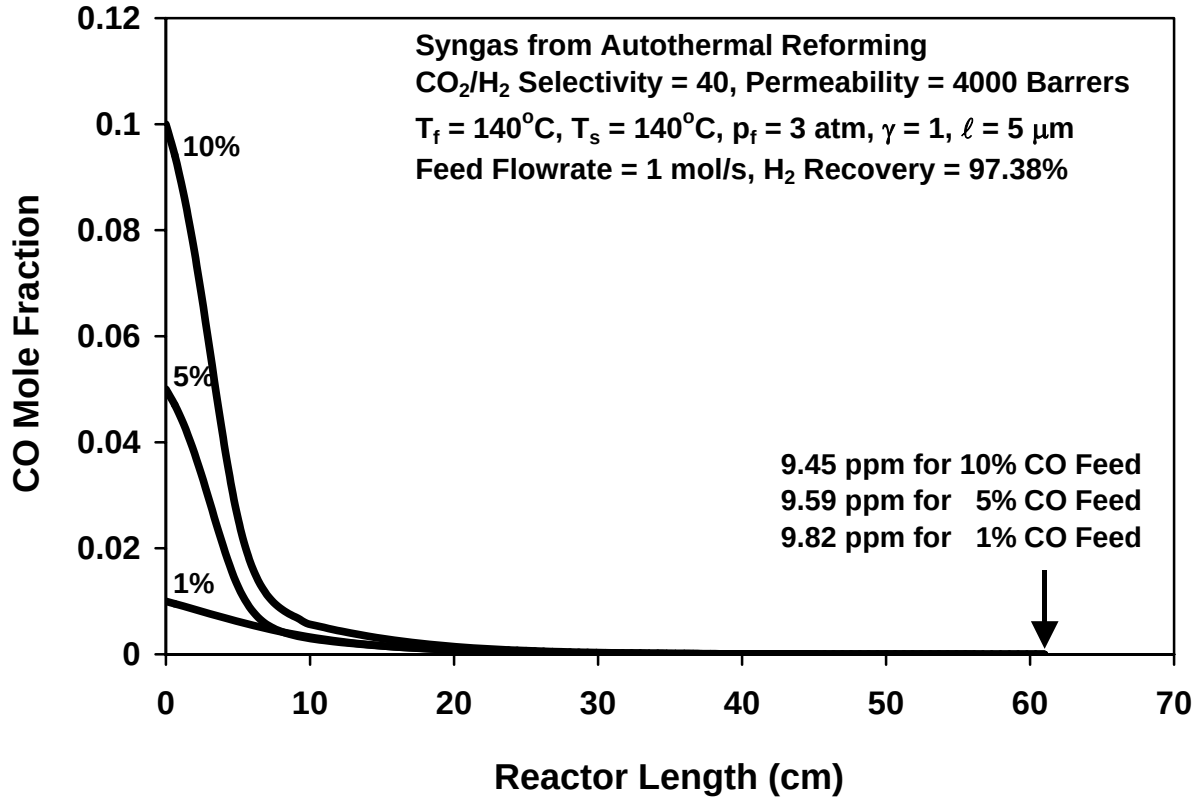

Figure 31. Feed-side CO mole fraction profiles along the length of membrane reactor for autothermal reforming syngases with 10%, 5%, and 1% CO.

For each of these synthesis gases, significant H_2 enhancement was achieved via CO_2 removal. For example, the H_2 concentration was increased from 41% in the inlet 1% CO feed gas to 49.3% in the outlet H_2 product on the wet basis including water (from 45.3% to 55.0% on the dry basis). Similar significant H_2 enhancement was also achieved for the 5% and 10% CO feed gases. In addition, a high H_2 recovery of greater than 97.3% was obtained for these synthesis gases as indicated in Figure 31.

We also investigated the effects of CO_2/H_2 selectivity on exit CO concentration and H_2 recovery for these synthesis gases through the modeling. For the CO_2/H_2 selectivity ranging from 10 to 80, the exit CO concentration of less than 10 ppm was achievable. A lower selectivity actually resulted in a slightly lower exit CO concentration as a lower selectivity (higher H_2 loss) enhanced the WGS reaction. However, the selectivity had a significant effect on H_2 recovery as shown earlier in Figure 10 for the 1% CO feed gas. A selectivity of 10 gave a H_2 recovery of about 90%, which is still quite good. As the selectivity increased, the H_2 recovery increased significantly. At the selectivity of 40, the H_2 recovery was greater than 97.3% as mentioned earlier. For the selectivity of 60 or greater, the H_2 recovery was greater than 98.2%.

We also did the same modeling study for the steam reforming syngases containing CO at concentrations of 10%, 5%, and 1%. Similar promising results on exit CO concentration and H_2 recovery were obtained. Figure 32 shows feed-side CO mole fraction profiles along the length of

membrane reactor for the steam reforming syngases with these inlet feed CO concentrations. For all these syngases, the H_2 products with <10 ppm CO were achieved.

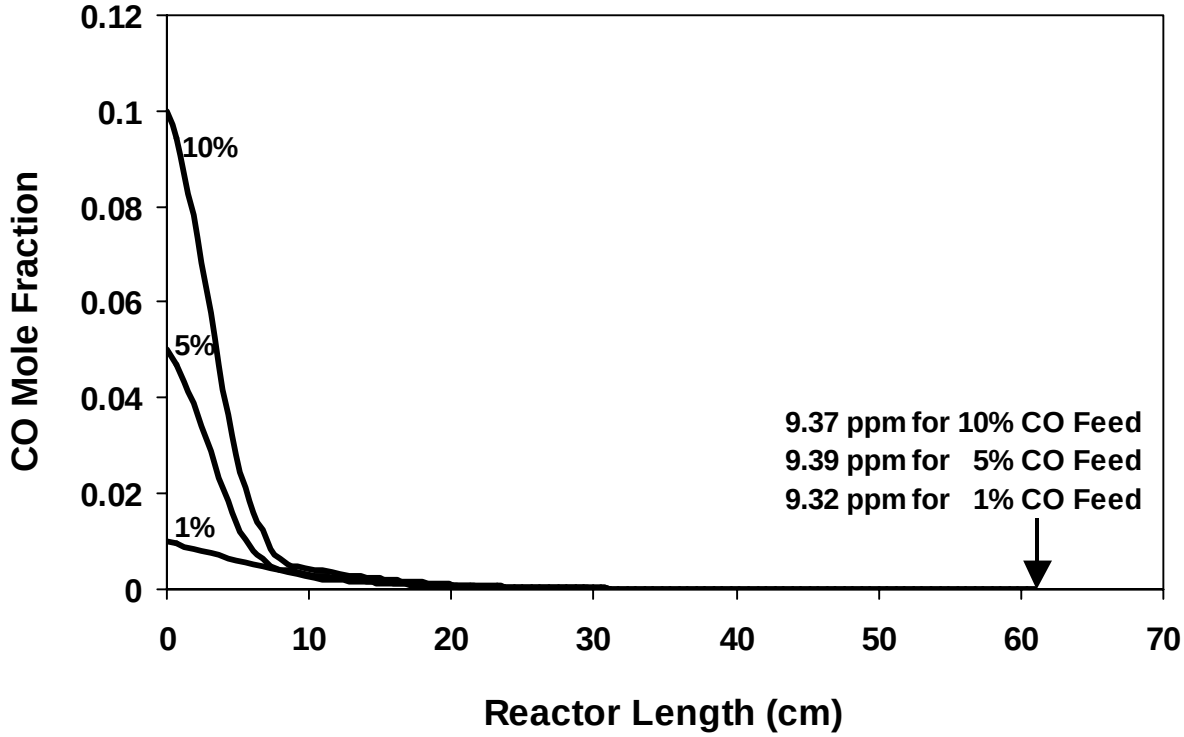

Figure 32. Feed-side CO mole fraction profiles along the length of membrane reactor for steam reforming syngases with with 10%, 5%, and 1% CO.

Laboratory Membrane Reactor ("Small Cell") Experiments

We studied and conducted the water gas shift (WGS) experiments using the laboratory WGS membrane reactor ("Small Cell", a circular cell) with the synthesis gas feed containing 1% CO (from autothermal reforming). The rationales for this CO level are two-fold: (1) it can be readily produced from commercial WGS reactors and (2) it requires CO_2 removal for its reduction via WGS reaction. In the membrane reactor experiments, the commercial Cu/ZnO catalyst supported on alumina was placed on the top of the membrane. The catalyst was activated / conditioned at 150^{o}C and 2.1 atm first with the gas of 1% H_2, 3% CO_2, 3% N_2, and 93% He for 6.1 hours and then with the gas of 40% H_2, 20% CO_2, and 40% N_2 until the CO concentration reached about 80 ppm (about 7.5 hours). Figure 33 shows H_2 and CO concentrations monitored during the catalyst activation using the gas of 40% H_2, 20% CO_2, and 40% N_2.

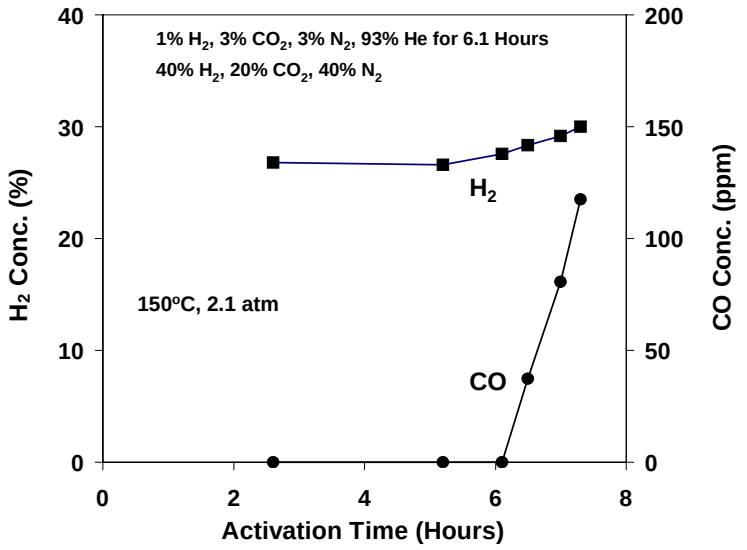

Figure 33. H_2 and CO concentrations monitored during the catalyst activation for the laboratory water-gas-shift membrane reactor ("Small Cell").

After the catalyst activation, the synthesis gas feed containing 1% CO, 17% CO_2, 45% H_2, 37% N_2 (on the dry basis) was admitted into the membrane reactor. The operating temperature was 150°C, and the feed pressure of the synthesis gas was 2.1 atm. Figure 34 summarizes all data obtained from this laboratory WGS membrane reactor ("Small Cell"). As shown in this figure, the CO concentration in the exit stream, i.e., the H_2 product, was <10 ppm (on the dry basis) for the various feed flow rates of the syngas at 6, 20, 30 and 40 cc/min under various feed water concentrations ranging from 15% to 70%. Even at the high feed rate of 60 cc/min, the CO concentration in the exit stream was very close to 10 ppm at the feed water concentration of about 45%.

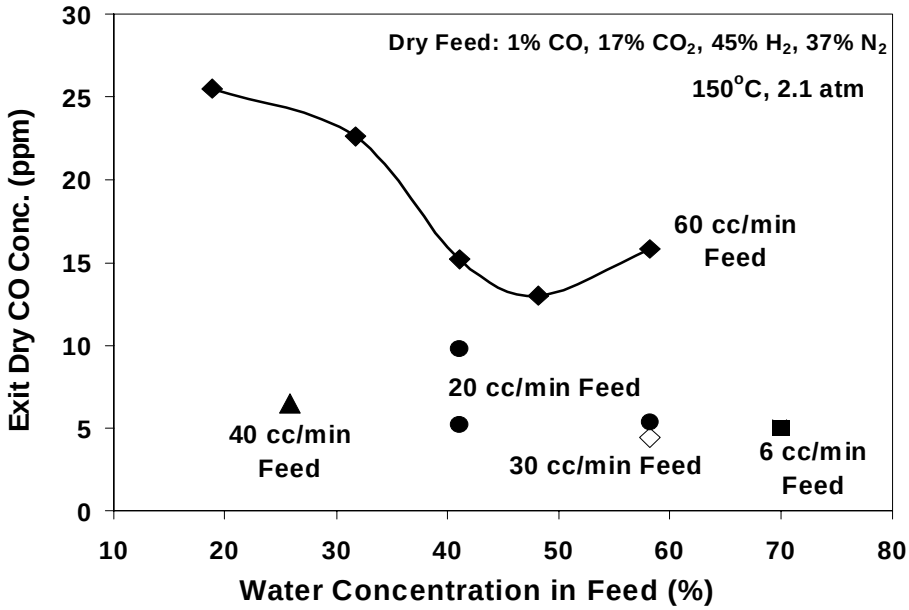

Figure 34. The results of CO in the H_2 product for the inlet 1% CO feed gas at various flow rates from the laboratory water-gas-shift membrane reactor ("Small Cell").

"Big Cell" Membrane Reactor Experiments

We constructed and set up a "Big Cell" membrane reactor for the scale-up of WGS membrane reactor. The "Big Cell" membrane reactor was a rectangular cell with a well-defined gas flow and velocity both for the feed and sweep sides. Thus, this membrane reactor was suitable for modeling and scale-up work. That is, the data from this membrane reactor can be used for comparison with modeling results and for scale-up. Figure 35 shows the schematic of this membrane reactor. This membrane reactor had 7.5 times the membrane area of the laboratory membrane reactor ("Small Cell").

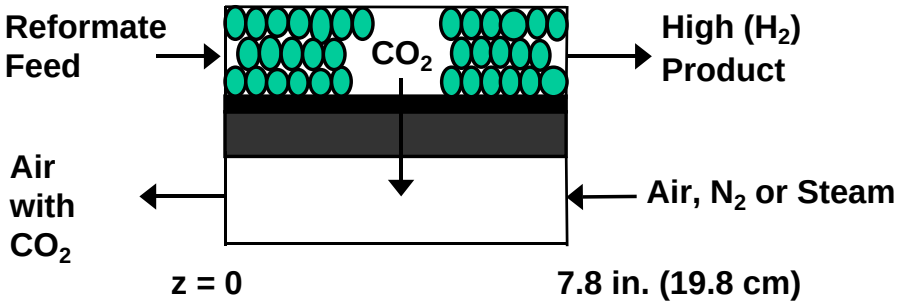

Figure 35. The schematic of the rectangular "Big Cell" water-gas-shift membrane reactor.

In the membrane reactor experiments using the "Big Cell", the similar way of the catalyst activation described earlier for the "Small Cell" membrane reactor was used. The catalyst in the "Big Cell" membrane reactor was activated / conditioned at 150^{o}C and 2 atm first with the gas of 1% H_2, 3% CO_2, 3% N_2, and 93% He for 6.2 hours and then with the gas of 40% H_2, 20% CO_2, and 40% N_2 until the CO concentration reached about 80 ppm (about 11.5 hours). Figure 36 shows H_2 and CO concentrations monitored during the catalyst activation using the gas of 40% H_2, 20% CO_2, and 40% N_2.

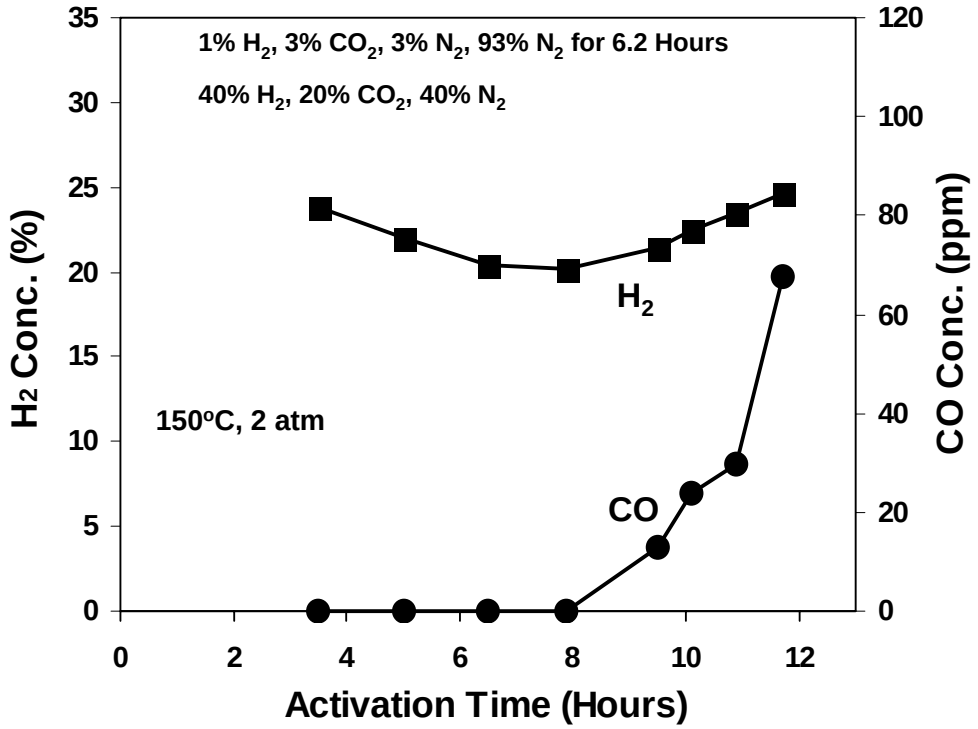

Figure 36. H_2 and CO concentrations monitored during the catalyst activation for the "Big Cell" water-gas-shift membrane reactor.

After the catalyst activation, the synthesis gas feed containing 1% CO, 17% CO_2, 45% H_2, 37% N_2 (on the dry basis) entered into the membrane reactor. The operating temperature was 150°C, and the feed pressure of the synthesis gas was 2 atm. Figure 37 shows the results obtained from this "Big Cell" WGS membrane reactor. As shown in this figure, the CO concentration in the exit stream, i.e., the H_2 product, was <10 ppm (on the dry basis) for the various feed flow rates of the syngas from 20 to 70 cc/min. The data agreed reasonably with the prediction by the non-isothermal mathematical model that we have developed [10-12] based on the material and energy balances, membrane permeation, and the low-temperature WGS reaction kinetics for the commercial catalyst ($Cu/ZnO/Al_2O_3$) reported by Moe [13] and Keiski et al. [14] as described earlier.

As indicated from Figure 17, if the feed pressure of the synthesis gas was higher than 2 atm, a higher feed gas rate could be processed to obtain <10 ppm CO in the H_2 product for the given membrane area of the "Big Cell" reactor.

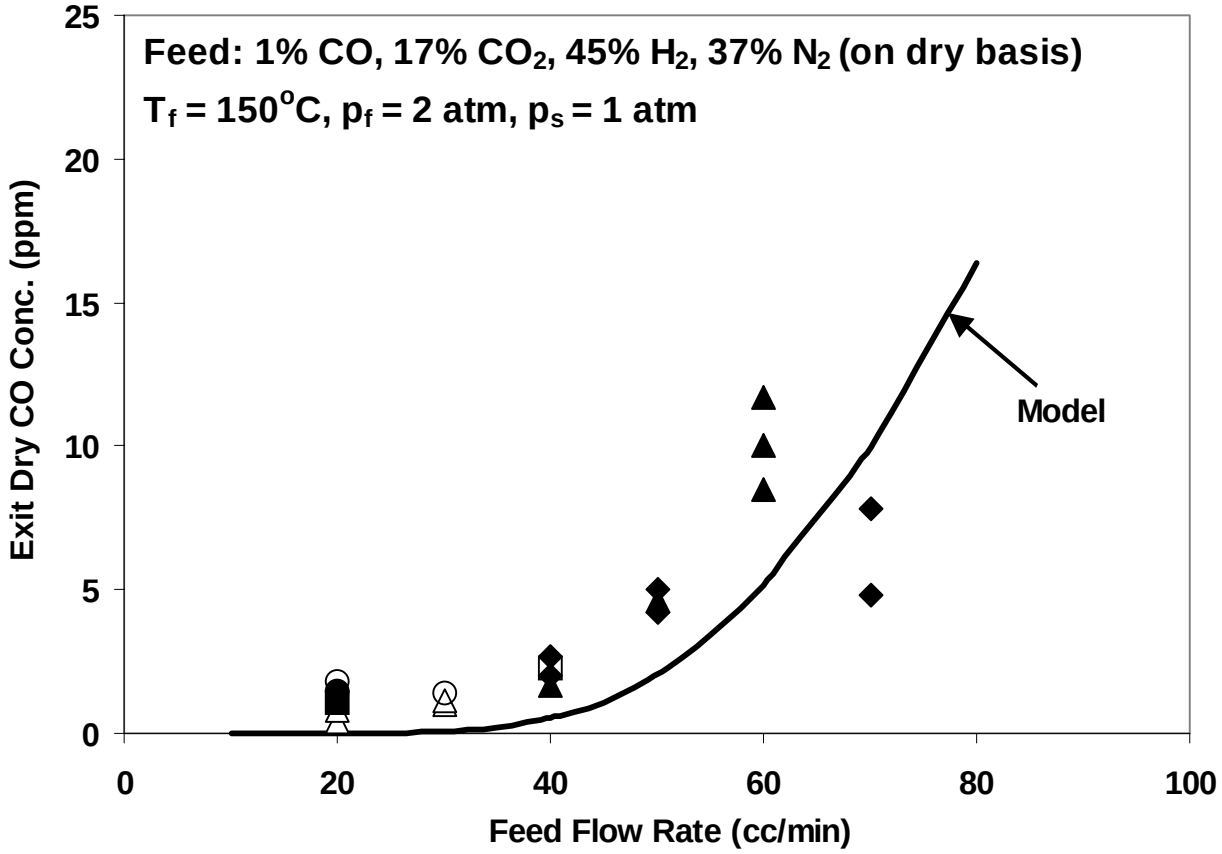

Figure 37. The results of CO in the H_2 product for the inlet 1% CO feed gas at various flow rates from the "Big Cell" water-gas-shift membrane reactor.

Gas hourly space velocity (GHSV) is defined in the following equation:

$$GHSV = \frac{Gas\ Flow\ Rate\ (\mathrm{L/h})}{Reactor\ Volume\ (\mathrm{L})} \tag{13}$$

Thus, the units of GHSV are hr^{-1}. The GHSV values for the data shown in Figure 37 were calculated according to this equation by taking into account the membrane thickness and packing density. The calculated GHSV results corresponding to the experimental data given in Figure 37 are shown in Figure 38. As shown in Figure 38, a high GHSV of about 4600 hr^{-1} is achievable. As mentioned earlier, if the feed pressure of the synthesis gas was higher than 2 atm, a higher feed gas rate could be processed, i.e., a higher GHSV would be achievable.

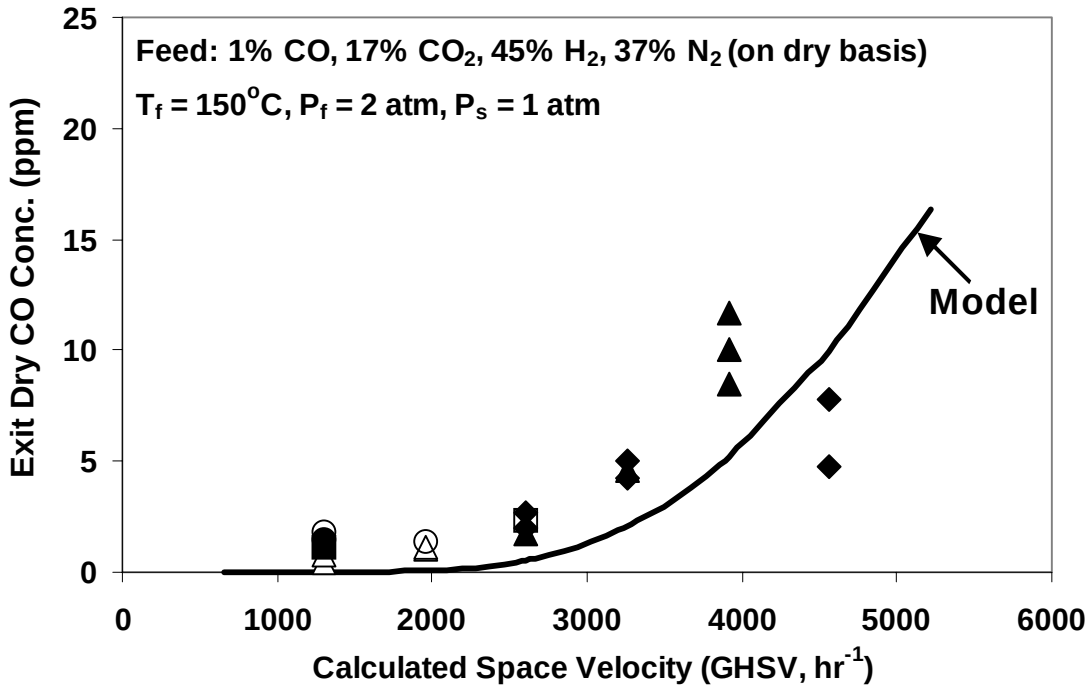

Figure 38. The calculated GHSV results for the data shown in Figure 37 at various flow rates from the "Big Cell" water-gas-shift membrane reactor.

Effective Removal of CO_2 from Syngas

The "Big Cell" without containing catalyst particles was also used for the removal of CO_2 from the same syngas (1% CO, 17% CO_2, 45% H_2, 37% N_2 (on the dry basis)). Figure 39 shows the schematic of this "Big Cell" for CO_2 removal experiments and modeling work.

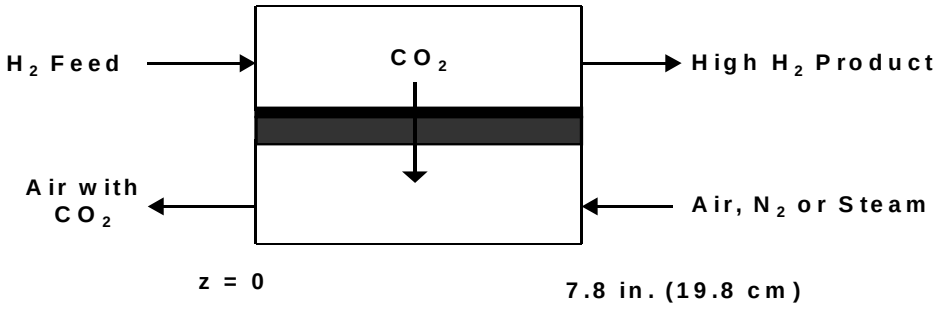

Figure 39. The schematic of the "Big Cell" without containing catalyst particles for CO_2 removal.

The membrane we synthesized was also used for the removal of CO_2 from this syngas using nitrogen as the sweep gas at the sweep / feed molar ratio of 1. Figure 40 depicts the results of CO_2 concentration (on the dry basis) in the exit stream (the H_2 product) at 120°C and 2 atm from the rectangular membrane cell at various feed flow rates. As depicted in this figure, a low CO_2 concentration of about 30 ppm was obtained for a feed flow rate of about 20 cc/min, indicating a nearly complete removal of CO_2 from the syngas. Even at the high feed rate of 110 cc/min, the CO_2 concentration in the exit stream was less than 1000 ppm (0.1%). Using steam instead of nitrogen as the sweep gas also gave similar, good results. Also shown in this figure, the data are in good agreement with the model that we have developed [10-12] based on the material and energy balances, and membrane permeation.

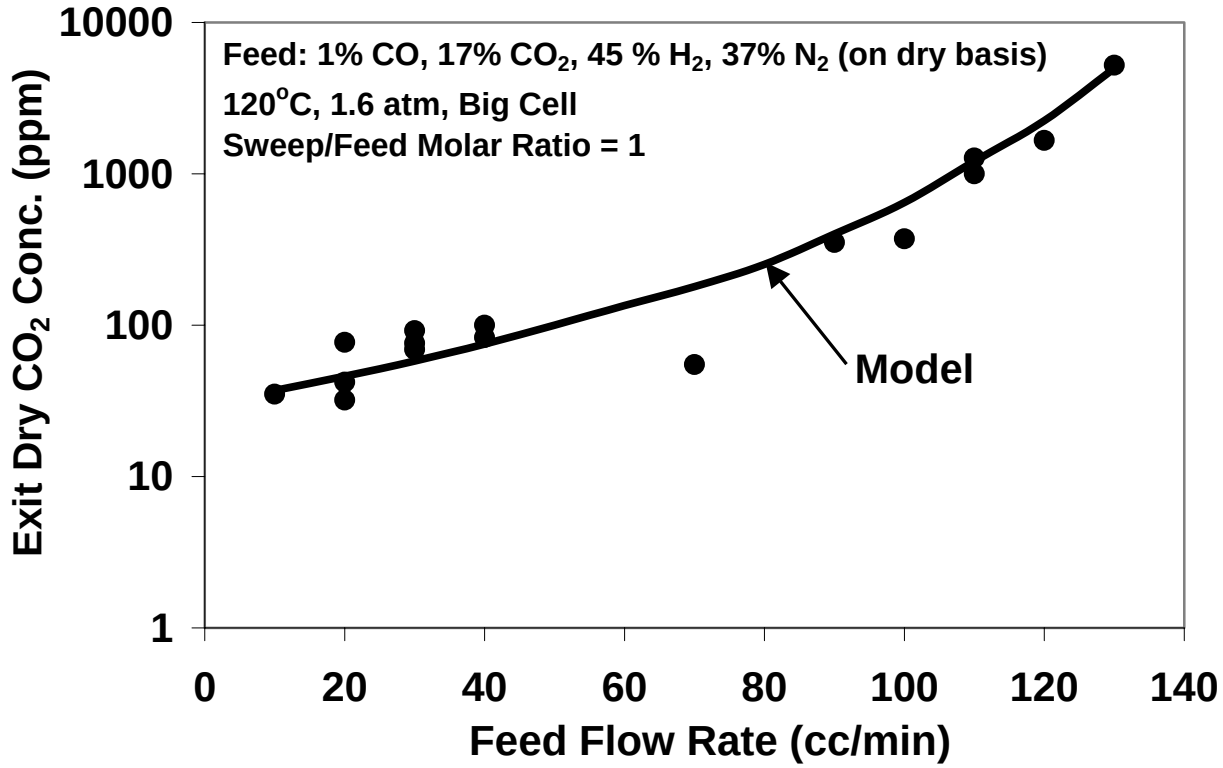

Figure 40. The results of the CO_2 concentration in the exit stream (the H_2 product) from the "Big Cell" (without containing catalyst particles) for the syngas feed with 1% CO and 17% CO_2 at various flow rates.

The GHSV values for the data shown in Figure 40 were calculated in the same way described earlier. The calculated GHSV results corresponding to the experimental data given in Figure 40 are shown in Figure 41. As shown in Figure 41, a high GHSV of about 11000 hr^{-1} is achievable for an exit CO_2 concentration of 0.1%.

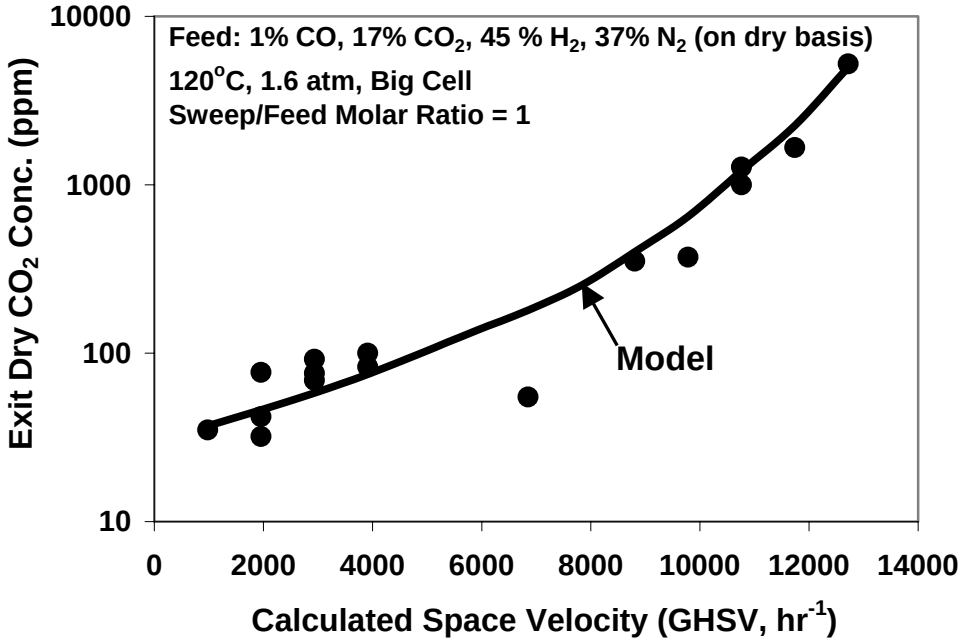

Figure 41. The calculated GHSV results for the data shown in Figure 40 from the "Big Cell" (without containing catalyst particles) for the syngas feed with 1% CO and 17% CO_2 at various flow rates.

Methanation of Treated Syngas to Achieve <10 ppm CO

The treated syngas with such a low CO_2 concentration of ~0.1% can be readily processed to convert the carbon oxides to methane via methanation at 160 – 220°C with a CO concentration of less than 10 ppm in the H_2 product [27-31]. The methanation reactions are as follows:

$$CO + 3\,H_2 \rightarrow CH_4 + H_2O \quad (14)$$

$$CO_2 + 4\,H_2 \rightarrow CH_4 + 2\,H_2O \quad (15)$$

As shown in equation (15), each mole of CO_2 takes 4 moles of H_2 to convert it to CH_4. Thus, it is important to remove CO_2 as much as possible before methanation in order to minimize the consumption of H_2. As shown in Figures 40 and 41, the membrane synthesized was very effective for the CO_2 removal before methanation.

Two types of methanation catalysts were used, one was Süd-Chemie C13-LT (0.3 wt% ruthenium on Al_2O_3 support) purchased from Süd-Chemie Inc., and the other was UNICAT MC-750 (NiO 65% on Al_2O_3 support) donated by UNICAT Catalyst Technologies Inc. [32, 33]. A piece of ¼ inch Inconel tubing was used as the methanation reactor. Catalyst particles were crashed into powders and loaded into the reactor. Gas flow was downward, and the gas flow rate was controlled by using a mass flow meter. Gas chromatograph (Agilent 6890N) was used to analyze gas compositions. Two thermal conductivity detectors (TCD) were used with argon and helium as the carrier gases, respectively.

Effects of Catalyst Activation

Both ruthenium and nickel catalysts need activation before use. Activation could be done at 180 to 350°C either with the process gas of 0.1% CO_2, 1.19% CO, 53.87% H_2, and 44.84% N_2 or a H_2/N_2 mixture gas. We have found that the activation method has significant effects on the methanation results. For Süd-Chemie C13-LT ruthenium catalyst, two different temperatures, 220 and 240°C, were used to activate the catalyst with the process gas. Figures 42 and 43 show the changes of CO, CH_4, and CO_2 during the activations at these two temperatures, respectively.

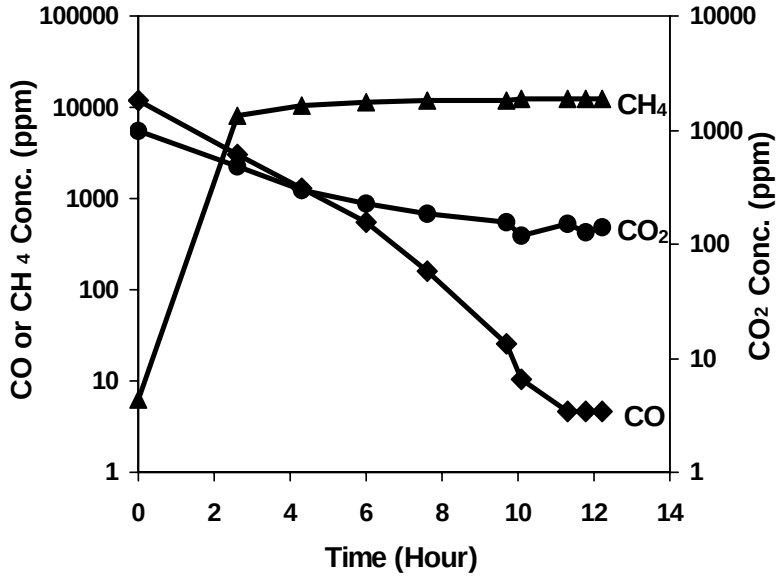

Figure 42. Outlet gas compositions during activation for Methanation Experiment M-1 at 220°C and 2 atm.

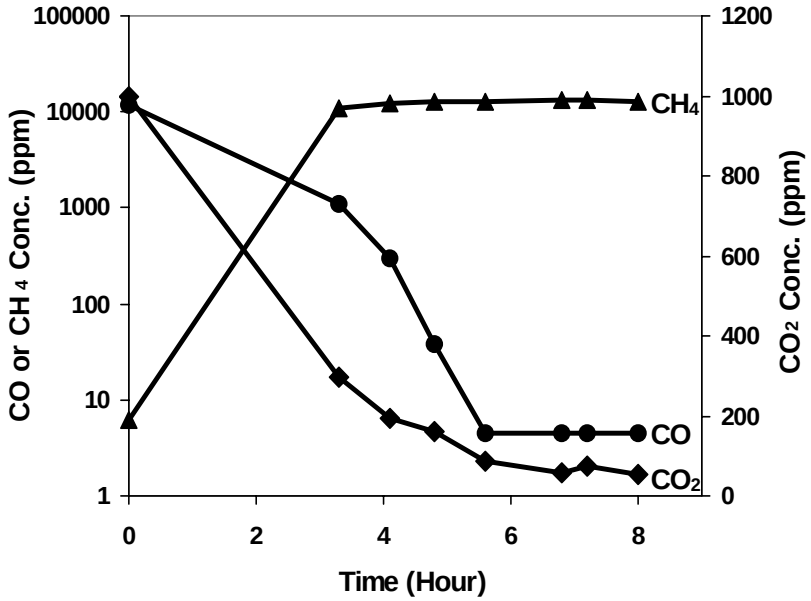

Figure 43. Outlet gas compositions during activation for Methanation Experiment M-2 at 240°C and 2 atm.

As shown in Figures 42 and 43, the CO concentration dropped faster at 240°C than at 220°C. The effects of activation on the methanation results are illustrated in Table 2. Both CO and CO_2 conversions with the activation at 240°C were better than those at 220°C.

Table 2. The effects of activation on methanation results at 200 and 210°C.

Activation	T (°C)	GHSV (hr^{-1})	Retentate Composition			
			H_2 (%)	CO (ppm)	CH_4 (%)	CO_2 (ppm)
M-1 (Activated at 220°C for 12.2 hours)	200	1200	50.66	7625	0.175	787.5
	210	1200	49.51	6272	0.335	798.3
M-2 (Activated at 240°C for 8.3 hours)	200	1154	48.43	5330	0.371	768.8
	210	1154	47.96	1606	0.821	785.2

During the activation, using the process gas or a H_2/N_2 mixture gas also showed some effects. In Methanation Experiment M-3 using the gas mixture of 40% H_2 and 60% N_2 for activation, the material balance particularly for H_2 was not as good as that for Methanation Experiment M-2 using the process gas for activation as shown in Table 3.

Table 3. The effects of activation using different gas on methanation results at 200°C.

Activation	T (°C)	GHSV (hr^{-1})	Retentate Composition			
			H_2 (%)	CO (ppm)	CH_4 (%)	CO_2 (ppm)
M-2 (Activated at 240°C for 8.3 hours with the process gas)	200	1154	48.43	5330	0.371	768.8
M-3 (Activated at 290°C with 40% H_2 and 60% N_2 at GHSV = 1154 h^{-1} for 15.7 hours and at GHSV = 2308 h^{-1} for 7.3 hours)	200	1154	34.82	2274	0.166	871.0

Effects of Catalyst

Both the ruthenium catalyst and the nickel catalyst are commercially available, but the nickel catalyst is the most widely used catalyst in industrial methanation. In our experiments, we found

that the ruthenium catalyst was more active than the nickel catalyst as indicated in Table 4 for methanation at 200°C and 2 atm.

Table 4. The effects of catalyst on methanation results at 200°C.

Activation	Catalyst Weight (g)	GHSV (hr^{-1})	Retentate Composition			
			H_2 (%)	CO (ppm)	CH_4 (%)	CO_2 (ppm)
M-3 (Süd-Chemie C13-LT (0.3 wt% ruthenium on Al_2O_3) activated at 290°C with 40% H_2 and 60% N_2 at GHSV = 1154 h^{-1} for 15.7 h and at GHSV = 2308 h^{-1} for 7.3 h)	1.498	1154	34.82	2274	0.166	871
M-4 (UNICAT MC-750 (NiO 65%, Balance Al_2O_3) activated at 290°C with 40% H_2 and 60% N_2 at GHSV = 3090 h^{-1} for 15.7 h)	1.417	1545	37.38	10382	0.016	1226

Effects of Temperature

The methanation reactions in equations (14) and (15) are strongly exothermic. The CO and CO_2 equilibrium constants, expressed in equations (16) and (17), respectively, are very large in the temperature range of 200 to 260°C, although they decrease as temperature goes up. The equilibrium constants are shown in Table 5 for 200 – 260°C. However, the reaction rate increases significantly as temperature goes up. In our experiments, CO and CO_2 conversions all showed sharp increases as temperature increased at 2 atm as illustrated in Table 6.

$$K_{P(CO)} = P_{CH4} P_{H2O} / P_{CO} P_{H2}^3 \tag{16}$$

$$K_{P(CO2)} = P_{CH4} P_{H2O}^2 / P_{CO2} P_{H2}^4 \tag{17}$$

Table 5. Equilibrium constants for methanation [33].

T (°C)	$K_{P(CO)}$	$K_{P(CO2)}$
200	0.215×10^{12}	0.947×10^{9}
220	0.235×10^{11}	0.156×10^{9}
240	0.304×10^{10}	0.294×10^{8}
260	0.456×10^{9}	0.627×10^{7}

Table 6. The effects of temperature on methanation results*.

T (^oC)	GHSV (hr^{-1})	Retentate Composition			
		H_2 (%)	CO (ppm)	CH_4 (%)	CO_2 (ppm)
200	1154	48.43	5330	0.371	768.8
210	1154	47.96	1606	0.821	785.2
240	1154	46.84	<4.6	1.305	63.25

*Methanation Experiment M-2 (Süd-Chemie C13-LT (0.3wt% ruthenium on Al_2O_3 support) activated at 240^{o}C for 8.3 hours with the process gas).

As shown in Table 6, at 240^{o}C, the CO concentration in the H_2 product was below the GC detection limit of 4.6 ppm. This suggested that <10 ppm CO in the H_2 product might be achievable with a lower temperature, e.g., 220^{o}C. Indeed, a result of <5 ppm CO was achieved at 220^{o}C for a gas hourly space velocity of 1442 hr^{-1} as shown in Table 7.

Effects of Flow Rate

The effects of process gas flow rate on methanation results at 220^{o}C are shown in Table 7. The process gas flow rate corresponding to a gas hourly space velocity of 1731 hr^{-1} gave an outlet CO concentration of 4.6 ppm. At a gas hourly space velocity of 1731 hr^{-1}, however, the flow rate seemed to be higher than the capacity of the catalyst, resulting in a CO concentration of 649.9 ppm.

Table 7. The effects of flow rate on methanation results*.

T (^oC)	GHSV (hr^{-1})	Retentate Composition			
		H_2 (%)	CO (ppm)	CH_4 (%)	CO_2 (ppm)
220	1442	48.66	4.6	1.168	564.3
220	1731	49.46	649.9	0.978	796.0

*Methanation Experiment M-2 (Süd-Chemie C13-LT (0.3wt% ruthenium on Al_2O_3 support) activated at 240^{o}C for 8.3 hours with the process gas).

Conclusions

We have synthesized membranes containing amino groups with high CO_2 permeabilities and high CO_2/H_2 and CO_2/CO selectivities. The membranes showed a high CO_2 permeability of about 4000 Barrers, a high CO_2/H_2 selectivity of greater than 40, and a high CO_2/CO selectivity of greater than 215 at 100 – 150^{o}C. These membranes could be operated to about 180^{o}C.

A one-dimensional non-isothermal model was developed to predict the performance of the novel water-gas-shift (WGS) membrane reactor. The modeling results have shown that H_2 enhancement (>99.6% H_2 for the steam reforming of methane and >54% H_2 for the autothermal reforming of gasoline with air on a dry basis) via CO_2 removal and CO reduction to 10 ppm or lower are achievable for synthesis gases. With this model, we have elucidated the effects of

system parameters, including CO_2/H_2 selectivity, CO_2 permeability, sweep/feed flow rate ratio, feed temperature, sweep temperature, feed pressure, catalyst activity, and feed CO concentration, on the membrane reactor performance. Both autothermal reforming and steam reforming syngases showed similar trends with respect to the system parameters. As the CO_2/H_2 selectivity increased, the recovery of H_2 increased, without affecting the membrane area requirement and the low CO attainment significantly. Higher membrane permeability resulted in the reduction of the required membrane area. Increasing sweep-to-feed ratio enhanced the permeation driving force but decreased the feed side temperature and thus the reaction rate, resulting in a net effect balanced between them and an optimal ratio of about 1. As either of the inlet feed and sweep temperatures increased, the membrane area requirement decreased. However, the temperatures greater than about 170°C would be unfavorable to the exothermic, reversible WGS reaction. Increasing feed pressure decreased the required membrane area significantly, particularly from 2 to 4 atm. Increasing catalyst activity enhanced WGS reaction and CO_2 permeation. The modeling study showed that both WGS reaction and CO_2 permeation played an important role on the overall reactor performance and that the reactor was effective for the syngases with a wide range of CO concentration (from 1% to at least 10%).

Based on the modeling study using the membrane data obtained, we showed the feasibility of achieving H_2 enhancement via CO_2 removal, CO reduction to $\leq$ 10 ppm, and high H_2 recovery. We obtained <10 ppm CO in the H_2 product in WGS membrane reactor experiments using the small circular laboratory membrane cell ("Small Cell") with the synthesis gas feed at a relatively low pressure of 2 atm with 1% CO. We confirmed the <10 ppm CO result using the "Big Cell" WGS membrane reactor with well-defined flow that had 7.5 times the area of "Small Cell". In other words, we have achieved the project milestone of <10 ppm CO in the H_2 product. The data from the "Big Cell" WGS membrane reactor agreed well with the mathematical model developed, which can be used for scale-up.

In addition, we removed CO_2 from a syngas containing 17% CO_2 to about 30 ppm. The CO_2 removal data agreed well with the mathematical model developed. The syngas with about 0.1% CO_2 and 1% CO was processed to convert the carbon oxides to methane via methanation to obtain <5 ppm CO in the H_2 product. Our methanation experiments showed that the ruthenium catalyst was more active than the common nickel based catalyst. The catalyst activation and the methanation temperature were very critical for CO and CO_2 conversions.

Nomenclature

c_p heat capacity (J/mol/K)
d hollow fiber diameter (cm)
d_h hydraulic diameter (cm)
h convective heat transfer coefficient ($W/cm^2/s$)
ΔH_r heat of reaction (J/mol)
J permeation flux ($mol/cm^2/s$)
k_a gas thermal conductivity (W/cm/s)
k_m membrane thermal conductivity (W/cm/s)
K_T reaction equilibrium constant (atm^{-2})
ℓ membrane thickness (cm)

L length of reactor or hollow fiber (cm)
n molar flow rate (mol/s)
Nu Nusselt number
p pressure (atm)
P permeability (Barrer)
Pr Prandtl number
r volumetric reaction rate (mol/cm^3/s)
R ideal gas constant (atm • cm^3/mol/K)
Re Reynolds number
Sc Schmidt number
Sh Sherwood number
T temperature (^{o}C)
U_i overall heat transfer coefficient (W/cm^2/K)
x feed side molar fraction
y sweep side molar fraction
z axial position along the length of reactor (cm)

Greek Letters

α CO_2/H_2 selectivity
γ inlet sweep-to-feed molar flow rate ratio
ε porosity of the support layer in the hollow fiber
ρ_b catalyst bulk density (g/cm^3)

Subscripts

0 initial
f feed side
i species
in inside of the hollow fiber
out outside of the hollow fiber
s sweep side
t total

References

1. W. S. W. Ho, "Membranes Comprising Salts of Aminoacids in Hydrophilic Polymers," U. S. Patent 5,611,843 (1997).

2. W. S. W. Ho, "Membranes Comprising Aminoacid Salts in Polyamine Polymers and Blends," U. S. Patent 6,099,621 (2000).

3. D. Lee, P. Hacarlioglu, and S. T. Oyama, "The Effect of Pressure in Membrane Reactors: Trade-off in Permeability and Equilibrium Conversion in the Catalytic Reforming of CH_4 with CO_2 at High Pressure," Topics in Catal., 29, 45-57 (2004).

4. A. Basile, L. Paturzo, and F. Gallucci, "Cocurrent and Countercurrent Modes for Water Gas Shift Membrane Reactor," Catal. Today, 82, 275-281 (2003).

5. D. Ma and C. R. F. Lund, "Assessing High-Temperature Water-Gas Shift Membrane Reactors," Ind. Eng. Chem. Res., 42, 711-717 (2003).

6. A. Criscuoli, A. Basile, and E. Drioli, "An Analysis of the Performance of Membrane Reactors for the Water-Gas Shift Reaction Using Gas Feed Mixtures," Catal. Today, 56, 53-64 (2000).

7. A. Basile, A. Criscuoli, F. Santella, and E. Drioli, "Membrane Reactor for Water Gas Shift Reaction," Gas Sep. Purif., 10, 243-254 (1996).

8. S. Uemiya, N. Sato, H. Ando, and E. Kikuchi, "The Water Gas Shift Reaction Assisted by a Palladium Membrane Reactor," Ind. Eng. Chem. Res., 30, 585-589 (1991).

9. J. Zou, G. Shil, and W. S. W. Ho, "Carbon Dioxide-Selective Membranes for Hydrogen Purification and Gas Separation," Proceedings of the Topical Conference on Advanced Membrane-Based Separations at AIChE Annual Meeting, San Francisco, CA, Paper 74t (2003).

10. W. S. W. Ho, "Development of Novel WGS Membrane Reactor," Final Technical Report for the DOE Project Conducted at the University of Kentucky (September 2002).

11. J. Huang and W. S. W. Ho, "A Modeling Study of CO_2-Selective Water-Gas-Shift Membrane Reactor for Fuel Cell," Proceedings of the Topical Conference on Advanced Membrane-Based Separations at AIChE Annual Meeting, San Francisco, CA, Paper 171c (2003).

12. J. Huang, J. Zou, and W. S. W. Ho, "Carbon Dioxide-Selective Water-Gas-Shift Membrane Reactor: A Modeling Study for Fuel Cells," Proceedings of North American Membrane Society 2004 Annual Meeting, Honolulu, Hawaii, Keynote Lecture, pp. 197-198, June 26-30, 2004.

13. J. M. Moe, "Design of Water-Gas-Shift Reactors," Chem. Eng. Progr., 58, 33 (1962).

14. R. L. Keiski, O. Desponds, Y. F. Chang, and G. A. Somorjai, "Kinetics of the Water-Gas-Shift Reaction over Several Alkane Activation and Water-Gas-Shift Catalysts," Applied Catalysis A: General, 101, 317-338 (1993).

15. W. S. W. Ho and K. K. Sirkar, eds., Membrane Handbook, Chapman & Hall, New York (1992).

16. J. S. Campbell, "Influences of Catalyst Formulation and Poisoning on the Activity and Die-off of Low Temperature Shift Catalysts," Ind. Eng. Chem. Proc. Des. Develop., 9, 588-595 (1977).

17. E. Fiolitakis, U. Hoffmann, and H. Hoffmann, "Application of Wavefront Analysis for Kinetic Investigation of Water-Gas Shift Reaction," Chem. Eng. Sci., 35, 1021-1030 (1980).

18. T. Salmi and R. Hakkarainen, "Kinetic Study of Low-Temperature Water-Gas Shift Reactor over a Copper-Zinc Oxide Catalyst," Appl. Catal., 49, 285-306 (1989).

19. N. Amadeo and M. Laborde, "Hydrogen Production from the Low Temperature Water-Gas Shift Reaction: Kinetics and Simulation of the Industrial Reactor," Int. J. Hydrogen Energy, 20, 949-956 (1995).

20. M.-C. Yang and E. L. Cussler, "Designing Hollow-Fiber Contactors," AIChE J., 32, 1910-1916 (1986).

21. L. Dahuron and E. L. Cussler, "Protein Extractions with Hollow Fibers," AIChE J., 34, 130-136 (1988).

22. M. J. Costello, A. G. Fane, P. A. Hogan, and R. W. Schofield, "The Effect of Shell Side Hydrodynamics on the Performance of Axial Flow Hollow Fiber Modules," J. Membr. Sci., 80, 1-11 (1993).

23. J. Wu and V. Chen, "Shell-Side Mass Transfer Performance of Randomly Packed Hollow Fiber Modules," J. Membr. Sci., 172, 59-74 (2000).

24. F. Lipnizki and R. W. Field, "Mass Transfer Performance for Hollow Fiber Modules with Shell-Side Axial Feed Flow: Using an Engineering Approach to Develop a Framework," J. Membr. Sci., 193, 195-208 (2001).

25. L. F. Brown, "A Comparative Study of Fuels for On-Board Hydrogen Production for Fuel-Cell-Powered Automobiles," Int. J. Hydrogen Energy, 26, 381-397 (2001).

26. S. Ahmed and M. Krumpelt, "Hydrogen from Hydrocarbon Fuels for Fuel Cells," Int. J. Hydrogen Energy, 26, 291-301 (2001).

27. Sud-Chemie, Inc., "Applications of Methanation," www.sud-chemie.com (2004).

28. Johnson Matthely, "Methanation Catalysts for Hydrogen Production," www.jmcatalysts.com (2004).

29. M. V. Twigg, ed., Catalyst Handbook, Wolfe Publishing Ltd., London, England, 2nd edition (1989).

30. K. Ledjeff-Hey, J. Roes, and R. Wolters, "CO_2-Scrubbing and Methanation as Purification System for PEFC," J. Power Sources, 86, 556-561 (2000).

31. B. Jenewein, M. Fuchs, and K. Hayek, "The CO Methanation on Rh/CeO_2 and CeO_2/Rh Model Catalysts: A Comparative Study," Surface Sci., 532-535, 364-369 (2003).

32. Süd-Chemie Inc., Süd-Chemie C13-LT catalyst specification (2004).

33. UNICAT Catalyst Technologies Inc., UNICAT MC-750 catalyst specification (2004).

FY 2002 Presentations/Publications

1. L. El-Azzami and W. S. W. Ho, "Modeling of Water-Gas-Shift Membrane Reactors with a CO_2-Selective Membrane for Fuel Cells," AIChE Annual Meeting, Reno, NV, November 4 – 9, 2001.

2. W. S. W. Ho, "Engineering Membranes for Environmental and Energy Applications," Invited Talk at the Ohio State University, Columbus, OH, March 14, 2002.

3. W. S. W. Ho, "Engineering Membranes for Environmental and Energy Applications," Invited Talk at the Colorado State University, Fort Collins, CO, March 29, 2002.

FY 2003 Presentations/Publications

1. W. S. W. Ho, "Engineering Membranes for Environmental and Energy Applications," Invited Talk at the University of Illinois, Urbana, IL, September 24, 2002.

2. W. S. W. Ho, "Engineering Membranes for Environmental and Energy Applications," Invited Talk at Case Western Reserve University, Cleveland, OH, October 17, 2002.

3. L. El-Azzami and W. S. W. Ho, "Modeling of CO_2-Selective WGS Membrane Reactor for Fuel Cells," AIChE Annual Meeting, Indianapolis, IN, November 3 - 8, 2002.

4. W. S. W. Ho and Y. H. Tee, "CO_2-Selective Membranes Containing Mobile and Fixed Carriers," AIChE Annual Meeting, Indianapolis, IN, November 3 - 8, 2002.

5. W. S. W. Ho, "Engineering Membranes for Environmental and Energy Applications," Invited Talk at University of California, Riverside, CA, December 6, 2002.

6. W. S. W. Ho, "Development of Novel Water-Gas-Shift Membrane Reactor," Presentation to Freedom CAR Fuel Cell Tech Team, USCAR, Detroit, MI, March 19, 2003.

FY 2004 Presentations/Publications

1. J. Huang, J. Zou, and W. S. W. Ho, "Facilitated Transport Membranes for Environmental and Energy Applications," Proceedings of the International Symposium on Emerging Environmental Technology, Kwangju Institute of Science & Technology, Gwangju, Korea, pp. 32 – 38 (2003).

2. J. Zou, G. Shil, and W. S. W. Ho, "Carbon Dioxide-Selective Membranes for Hydrogen Purification and Gas Separation," Proceedings of the Topical Conference on Advanced Membrane-Based Separations at AIChE Annual Meeting, San Francisco, CA, Paper 74t (2003).

3. J. Huang and W. S. W. Ho, "A Modeling Study of CO_2-Selective Water-Gas-Shift Membrane Reactor for Fuel Cell," Proceedings of the Topical Conference on Advanced Membrane-Based Separations at AIChE Annual Meeting, San Francisco, CA, Paper 171c (2003).

4. W. S. W. Ho, "Facilitated Transport Membranes for Environmental and Energy Applications," Industrial Technology Research Institute, Energy & Resources Laboratories, Hsinchu, Taiwan, December 16, 2003.

5. W. S. W. Ho, "Facilitated Transport Membranes for Environmental and Energy Applications," Department of Chemical Engineering, National Taiwan University, Taipei, Taiwan, December 17, 2003.

6. W. S. W. Ho, "Fuel Cell and Membrane Technology: An Overview," Departments of Chemistry and Physics, Soochow University, Taipei, Taiwan, December 18, 2003.

7. W. S. W. Ho, "Facilitated Transport Membranes for Environmental and Energy Applications," Department of Chemical Engineering, Chung-Yuan University, Chung-Li, Taiwan, December 19, 2003.

8. W. S. W. Ho, "Engineering Membranes for Environmental and Energy Applications," HydrogenSource LLC, South Windsor, CT, February 25, 2004**.**

9. W. S. W. Ho, "Development of Novel CO_2-Selective Membrane for H_2 Purification," DOE Hydrogen, Fuel Cells & Infrastructure Technologies 2004 Program Review, Philadelphia, PA, Project No. 107, May 24-27, 2004.

10. W. S. W. Ho, "Development of Novel CO_2-Selective Membrane for H_2 Purification," Proceedings of DOE Hydrogen, Fuel Cells & Infrastructure Technologies 2004 Program Review, Philadelphia, PA, Project No. 107, Paper FC-P3, May 24-27, 2004.

11. J. Huang, J. Zou, and W. S. W. Ho, "Carbon Dioxide-Selective Water-Gas-Shift Membrane Reactor: A Modeling Study for Fuel Cells," North American Membrane Society 2004 Annual Meeting, Honolulu, Hawaii, Keynote Lecture, June 26-30, 2004.

12. J. Huang, J. Zou, and W. S. W. Ho, "Carbon Dioxide-Selective Water-Gas-Shift Membrane Reactor: A Modeling Study for Fuel Cells," Proceedings of North American Membrane Society 2004 Annual Meeting, Honolulu, Hawaii, Keynote Lecture, pp. 197-198, June 26-30, 2004.

13. W. S. W. Ho, "Carbon Dioxide-Selective Membranes for Hydrogen Purification from Syngas," Chung Yuan University and Yuan-Ze University, Chung-Li, Taiwan, July 7-9, 2004.

14. W. S. W. Ho, "Carbon Dioxide-Selective Membranes for Hydrogen Purification," GE Global Research Center, Niskayuna, NY, August 17, 2004.

15. W. S. W. Ho, "Carbon Dioxide-Selective Membranes for Hydrogen Purification from Syngas," Gas Technology Institute, Des Plaines, IL, August 20, 2004.

16. W. S. W. Ho, "Engineering Membranes for Environmental and Energy Applications," East China University of Science & Technology, Shanghai, China, September 1, 2004.

17. W. S. W. Ho, "Engineering Membranes for Environmental and Energy Applications," Zhejiang University, Hangzhou, China, September 15, 2004.

18. J. Huang, J. Zou, and W. S. W. Ho, "Engineering Membranes for Environmental and Energy Applications," 10th Congress of Asia Pacific Confederation of Chemical Engineering, Kitakyushu, Japan, Keynote Lecture, October 17-21, 2004.

19. J. Huang, J. Zou, and W. S. W. Ho, "Engineering Membranes for Environmental and Energy Applications," Proceedings of 10th Congress of Asia Pacific Confederation of Chemical Engineering, Kitakyushu, Japan, Keynote Lecture, Paper No. 3F-01, October 17-21, 2004.

20. J. Zou, J. Huang, and W. S. W. Ho, "Carbon Dioxide Removal with Polymer Membranes for Hydrogen Purification for Fuel Cells," AIChE Annual Meeting, Austin, TX, Paper No. 238v, November 7-12, 2004.

21. J. Huang, J. Zou, and W. S. W. Ho, "CO_2-Selective Water-Gas-Shift Membrane Reactor for Fuel Cells: A Modeling and Experimental Study," AIChE Annual Meeting, Austin, TX, Paper No. 238w, November 7-12, 2004.

22. J. Zou, J. Huang, and W. S. W. Ho, "Facilitated Transport Membranes for Environmental and Energy Applications," First India-USA Joint Chemical Engineering Conference, Mumbai, India, Keynote Lecture, December 28-30, 2004.

23. J. Zou, J. Huang, and W. S. W. Ho, "Facilitated Transport Membranes for Environmental and Energy Applications," Proceedings of First India-USA Joint Chemical Engineering Conference, Mumbai, India, Keynote Lecture, Paper No. 12.6.2, December 28-30, 2004.

24. J. Huang, L. El-Azzami, and W. S. W. Ho, "Modeling of CO_2-Selective Water-Gas-Shift Membrane Reactor for Fuel Cell," submitted to Journal of Membrane Science, 2004.

Special Recognitions & Awards/Patents

1. W. S. W. Ho, "CO_2-Selective Membranes Containing Amino Groups," U. S. Patent Application Serial No. 10/145,297, filed on May 14, 2002.

2. S. Randhava, W. S. W. Ho, Richard L. Kao, and E. H. Camara, "Dynamic Sulfur Tolerant Process and System with Inline Acid Gas-Selective Removal for Generating Hydrogen for Fuel Cells," U. S. Patent Application Serial Number 10/236,324, allowed (July, 2004).

3. W. S. W. Ho, "Membranes, Methods of Making Membranes, and Methods of Separating Gases Using Membranes," U.S. Provisional Patent Application, Reference No. 04ID129F, filed on November 5, 2004.

4. W. S. W. Ho, Perkin Elmers' Padmabhushan Professor R. Kumar Chemcon Distinguished Speaker Award for 2004, Indian Institute of Chemical Engineers (2004).

5. W. S. W. Ho, Keynote Speaker on "Carbon Dioxide-Selective Water-Gas-Shift Membrane Reactor: A Modeling Study for Fuel Cells," North American Membrane Society 2004 Annual Meeting, Honolulu, Hawaii, June 26-30, 2004.

6. W. S. W. Ho, Invited Keynote Speaker on "Engineering Membranes for Environmental and Energy Applications," 10th Congress of Asia Pacific Confederation of Chemical Engineering, Kitakyushu, Japan, Paper No. 3F-01, October 17-21, 2004.

7. W. S. W. Ho, Invited Keynote Speaker on "Facilitated Transport Membranes for Environmental and Energy Applications," First India-USA Joint Chemical Engineering Conference, Mumbai, India, Paper No. 12.6.2, December 28-30, 2004.

Acronyms

ppm - part per million (one PPM is equivalent to 0.0001%)
WGS - water gas shift